Monsoonal variations in aerosol optical properties and estimation of aerosol optical depth using ground-based meteorological and air quality data in Peninsular Malaysia

F. Tan[1], H. S. Lim[1], K. Abdullah[1], T. L. Yoon[1], and B. Holben[2]

[1]School of Physics, Universiti Sains Malaysia, 11800 Penang, Malaysia
[2]NASA Goddard Space Flight Center, Greenbelt, Maryland, USA

Correspondence to: F. Tan (fuyitan@yahoo.com)

Abstract

Obtaining continuous AOD measurements is a difficult task due to cloud cover problem. An AOD-predicting model with the main motivation to overcome this problem is proposed. In this study, the optical properties of aerosols in Penang, Malaysia were analyzed for four monsoonal seasons (northeast monsoon, pre-monsoon, southwest monsoon, and post-monsoon) based on data from the AErosol RObotic NETwork (AERONET) from February 2012 to November 2013. The aerosol distribution patterns in Penang for each monsoonal period were quantitatively identified according to the scattering plots of the Angstrom exponent against the aerosol optical depth (AOD). A new empirical algorithm was proposed to predict the AOD data. Ground-based measurements (i.e., visibility and air pollutant index) were used in the model as predictor data to retrieve the missing AOD data from AERONET due to frequent cloud formation in the equatorial region. The model coefficients were determined through multiple regression analysis using selected data set from in situ data. The calibrated model coefficients have a coefficient of determination, R^2, of 0.72. The predicted AOD of the model was generated based on these calibrated coefficients and compared against the measured data through standard statistical tests, yielding a R^2 of 0.68 as validation accuracy. The error in weighted mean absolute percentage error (wMAPE) was less than 0.40 % compared with the real data. The results revealed that the proposed model efficiently predicted the AOD data. Performance of our model was compared against selected LIDAR data to yield good correspondence. The predicted AOD can enhance measured short- and long-term AOD and provide supplementary information for climatological studies and monitoring aerosol variation.

1 Introduction

Air quality issues in Asia can be attributed to unavoidable climate change impacts and the negative impact of anthropogenic activities arising from rapid population growth, industrialization and urbanization (IPCC, 2007, 2013). Aerosol optical depth (AOD) derived from remote sensing has potential for assessing air quality. In general, spatial and temporal variations in AOD data are large since they depend on production sources, transport and removal processes that are modulated by local and synoptic meteorological conditions. Many

small-scale studies on the optical properties of aerosols have been conducted by Chew et al. (2013); Mishra et al. (2013); Salinas et al. (2013) using sun and sky scanning radiometers of AErosol RObotic NETwork (AERONET) (Holben et al., 1998). These methods are limited spatially relative to satellite imagery, and therefore are complementary for comprehensive studies on atmospheric aerosols. Continuous measurements of AOD data are difficult because the atmosphere is frequently cloudy. To better monitor and understand aerosol variation, sufficient measurements and a practical observation paradigm of aerosols are necessary (Hansen et al., 1997; Tripathi et al., 2005; Kaskaoutis et al., 2007; Kaskaoutis and Kambezidis, 2008; Russell et al., 2010).

Southeast Asia (SEA) stands out globally as it hosts one of the most complex meteorological and environmental conditions, making remote sensing difficult both for AERONET and satellites (Reid et al., 2013). Cloud cleared data leave gaps in our remote sensing data record and conversely residual cloud contamination of remotely sensed data cause challenging tasks to scientists studying aerosols (Chew et al., 2011; Campbell et al., 2013). Moreover, anthropogenic biomass burning activities have increased dramatically in recent decades for land preparation and forest clearance (Field et al., 2009). These fire activities result in trans-boundary and long-range transport of aerosols that often affect air quality in both source and surrounding regions (Hyer and Chew, 2010; Reid et al., 2013; Salinas et al., 2013; Lin et al., 2014b). Those aerosols mix with locally generated aerosols (Engling et al., 2014). Therefore, it is potentially valuable to develop a regional/local model to estimate and monitor AOD.

Development of an empirical model to produce reliable AOD estimates for aerosol monitoring at local scales is novel and necessary for SEA, with potential global applications (Chen et al., 2013; Fan et al., 2013). Several researchers have used models as alternative tools to predict AOD values by using various ground based meteorology measurements (Wang et al., 2009; Qin et al., 2010; Lin et al., 2014a). However, this approach has not yet been applied over the Malay Peninsula region of SEA.

Previous studies indicate that AOD is proportional to air quality parameters such as particulate matter (PM) with diameters less than 10 or 2.5 μm (PM_{10} or $PM_{2.5}$) (Wang and Christopher, 2003; Cordero et al., 2012; Mielonen et al., 2012; Mogo et al., 2012; Müller et al., 2012) but inversely proportional to visibility (Vis) (Horvath, 1995; Li and Lu, 1997; Peppler et al., 2000; Bäumer et al., 2008; Singh and Dey, 2012) assuming most of the aerosol is at the surface. However, there are studies stating that AOD is not always highly correlated to surface or horizontal measurements especially with the occurrence of an elevated layer of AOD from transported dust or biomass burning (Mahowald et al., 2007; Barladeanu et al., 2012; Chen et al., 2013; Toth et al., 2014).

In this paper, our goal is to build on previous experience to develop an AOD prediction model based on three types of measured data, namely (i) RH, (ii) Vis and (iii) air pollution index (API). These parameters are measured routinely at many ground-based stations. The AOD prediction model based on these routine measurements is necessary to establish a long-term database for i) climatological studies, ii) providing continuous atmospheric columnar AOD data, and iii) monitoring aerosol variation such as diurnal cycles of AOD. Meanwhile, it is important to understand the source of and dominant type of aerosol in this study. There is an absence of understanding these factors on a local scale.

AOD measurements were obtained through the AERONET site located in Universiti Sains

Malaysia (USM) with geo-coordinates 5.36˚ N and 100.30˚ E. All AERONET direct sun data used were Level 2 quality assured (Smirnov et al., 2000). The Vis and API data were taken from the meteorological stations at the Penang International Airport and USM. All data were taken between 2012 and 2013. The aerosol characteristics in Penang are comprehensively analyzed for variation based on changes in seasonal monsoons. A near real-time AOD model is established based on multiple regression analysis of Vis and API. The accuracy and efficiency of the model are evaluated to assess air quality at Penang.

2 Methodology and statistical model

The present work was based on previous studies of Tan et al. (2014a, b). They predicted AOD using multiple regression analysis based on meteorological and air quality data. The AOD prediction model has been validated and successfully proven for the southwest monsoon period (June-September, 2012) in Penang Island, Malaysia. However, the following issues require reconciliation: (i) under- and overprediction of AOD were not assessed because of the lack of available LIDAR data to monitor the variations in the vertical profile of the aerosol distribution, (ii) the algorithm was insufficiently robust because only a four month dataset was considered; and (iii) seasonal changes other than southwest monsoon were not included in their study. The present study uses a two-year dataset (2012, 2013) at Penang to validate the algorithms proposed by Tan et al. (2014a, b).

Penang is an island located in the northwestern region of Peninsular Malaysia and lies within latitudes 5.20˚ N to 5.50˚ N and longitudes 100.15˚ E to 100.43˚ E (Fig. 4). The weather is warm and humid year-round. However, two main monsoon seasons exist, northeast and southwest monsoons. Considering previous analyses of aerosol and air quality (Awang et al., 2000; Krishna Moorthy et al., 2007; Suresh Babu et al., 2007; Kumar and Devara, 2012; Chew et al., 2013; Xian et al., 2013), the monsoon periods in this study were classified as follows: (i) northeast monsoon (December–March), (ii) transition period of northeast to southwest monsoon or pre-monsoon (April–May), (iii) southwest monsoon (June–September), and (iv) transition period of southwest to northeast monsoon or post-monsoon (October–November).

The AOD and Angstrom exponent are analyzed to identify the aerosol and broadly characterize properties in Penang during each period. Precipitable water (PW) was used to indicate the amount of the total water content in the atmosphere. The seasonal variations in AOD, Angstrom exponent, and PW based on frequency distribution patterns are identified. The aerosol types are seasonally discriminated from scatter plots of Angstrom exponent against the AOD. Threshold values in the scatter plot for aerosol classification have been previously reported by Smirnov (2002b, 2003), Pace et al. (2006), Kaskaotis (2007), Toledano et al. (2007), Salinas et al. (2009), and Jalal et al. (2012). The data selection criteria proposed by Tan et al. (2014a) are used in this study. Seasonal back-trajectory frequency plots from the Hybrid Single-Particle Lagrangian Integrated Trajectory (HYSPLIT_4) model are used to identify the frequency occurrence of origin sources for aerosol and transported pathways (Draxler and Hess, 1998; Wai et al., 2014).

AOD, API, and Vis data were selected according to the procedure of Tan et al. (2014a) to generate predicted AOD data. AOD is computed from the solar transmission measured at 340, 380, 440, 500, 675, 1020, and 1640 nm using the automatic tracking sun and sky scanning radiometers (Holben et al., 1998). These AOD data can be obtained from the AERONET web

page (http://aeronet.gsfc.nasa.gov). AERONET data has three different levels. Level 1.0 is cloud-unscreened data, and Level 1.5 is cloud-screened data. Only Level 2.0 was employed in this study because they are cloud screened and quality assured (Smirnov et al. 2000). Vis data were retrieved online from Weather Underground (http://www.wunderground.com) or from NOAA satellite (http://www7.ncdc.noaa.gov/CDO/cdo). Hourly data free from rainfall, thunderstorms, or fog during the calculations were utilized to predict AOD. Air quality in Malaysia is reported in terms of API, which can be obtained from the Department of Environment in Malaysia (http://apims.doe.gov.my/apims/). API is calculated from carbon monoxide, ozone, nitrogen dioxide, sulfur dioxide and PM_{10}. Malaysia is mainly polluted by PM_{10} (DOE, 2010). Therefore only API that are predominantly due to PM_{10} are used in this study. API is computed using the technique developed by US-EPA. The Malaysian Department of Environment provides a standardized procedure on how to calculate API values (DOE, 1997). The conversion between API and PM_{10} has been shown in the guideline provided in DOE (1997).

A total of 790 data points from 2012 to 2013 were used. Initially, the datasets were separated into five sets as follows: (i) northeast monsoon, (ii) pre-monsoon, (iii) southwest monsoon, (iv) post-monsoon and (v) annual dataset (overall). The number of data points for northeast monsoon, pre-monsoon, southwest monsoon and post-monsoon were 257, 132, 235, and 166 respectively. In a particular seasonal monsoon period there are n data, $\{D_1, D_2, D_3, D_4, D_5, \ldots D_n\}$, which are arranged sequentially in time. The data for each seasonal monsoon were further divided into two subsets, in the form of $\{D_1, D_3, D_5, \ldots\}$ and $\{D_2, D_4, D_6, \ldots\}$. The first data subset was used to calibrate (Eq. 1) for AOD at 500 nm, given below:

$$\mathrm{AOD} = a_0 + a_1(\mathrm{RH}) + a_2(\mathrm{RH})^2 + a_3(\mathrm{RH})^3 + a_4(\mathrm{Vis}) + a_5(\mathrm{Vis})^2 + a_6(\mathrm{Vis})^3 + a_7(\mathrm{API}) + a_8(\mathrm{API})^2 + a_9(\mathrm{API})^3 \quad (1)$$

where RH is the surface relative humidity (Tan et al., 2014a).

The root mean square error (RMSE), coefficient of determination (R^2), and weighted mean absolute percentage error (wMAPE) between the measured and predicted AOD for each seasonal model were calculated at 95 % confidence level. The wMAPE parameter was used to quantify the systematic differences between the concentration levels. This parameter is given as follows: $\mathrm{wMAPE} = (\sum |((\mathrm{AOD}_{p,i} - \mathrm{AOD}_{m,i})/\mathrm{AOD}_{m,i})| * \mathrm{AOD}_{m,i} / \sum \mathrm{AOD}_{m,i}) * 100$, where the subscript p refers to predicted, m to measured and i to individual measurements. The ability of the proposed model to produce reliable AOD estimates for temporal air quality monitoring can be quantitatively justified or falsified based on the value of the resultant wMAPE.

Aerosols can be hydrophilic or hydrophobic, and these properties can have a non-trivial impact on the magnitude of the retrieval AOD (Tang, 1996; Song et al., 2007; de Meij et al., 2012; Singh and Dey, 2012; Ramachandran and Srivastava, 2013; Wang et al., 2013; van Beelen et al., 2014). However, to discriminate between hydrophilic and hydrophobic aerosols requires additional resources beyond the reach of the present study. Most fine mode aerosols such as sulfates (that likely dominate urban industrial aerosol composition) are hygrophilic such that one would expect RH to exert a significant influence on the measured AOD. Given that Penang is dominated by urban industrial aerosols, one would expect RH to be an important variable in the model. However, our pre-analysis showed that RH does not contribute significantly to AOD prediction. We suggest that the RH, which is very high year around in Penang, exerts less influence on AOD than we would see in drier climates. If RH were considered as a predictor, its related factors (e.g., aerosol stratification (dust or smoke

aloft), convection, and hysteresis in particles) should otherwise be taken into account. The contribution of RH to the aerosol properties was integrated in the aerosol model of Srivastava et al., (2012), because the net effect of RH on aerosol and related factors were difficult to quantify. In similar spirit, the RH contribution is disregarded in the present model, yielding Eq. (2), given as follows:

$$AOD = a_0 + a_1(Vis) + a_2(Vis)^2 + a_3(Vis)^3 + a_4(API) + a_5(API)^2 + a_6(API)^3 \quad . \qquad (2)$$

RMSE, R^2, wMAPE were calculated for Eq. (2) in each monsoon season. The data for subset 1 (i.e., {D_1, D_3, D_5, …}) was used for calibration. The data for subset 2 ({D_2, D_4, D_6, …}) was used for cross-validation.

Lee et al. (2012) exclude days when the deviation between the measured and predicted values was greater than RMSE, or when the estimated AOD slope was negative because of measurement errors and cloud-contaminated AOD. The potential outliers in our model were removed following the approaches of Lee et al. (2012). The aforementioned procedures were used to calibrate the AOD prediction model, Eq. (2), using the resulting data from subset 1 after the elimination of outliers. The resultant coefficients of the calibration were then applied to data for subset 2 for cross validation, in which the predicted AOD values were compared with the measured data from AERONET.

Equation (2) was then applied to retrieve the AOD when no AOD values (from AERONET) were available. The under- and overpredicted AOD were examined using a RAYMETRICS LIDAR system if the data were available. Our LIDAR system is co-located with the CIMEL sunphotometer at the rooftop of School of Physics, USM (longitude 100.30° E, latitude 5.36° N). The detailed description of this LIDAR system can be found in articles written by Tan et al. (2013, 2014c). The LIDAR signals were pre-analyzed based on the protocol mentioned in Tan et al. (2013, 2014c). We shall briefly illustrate the protocol here. First, background solar radiation in the LIDAR signal has to be deducted. Then the analog and photon signals in the LIDAR signal are combined to enhance the near and far field signals. The range corrected signal (RCS) is obtained by multiplying the combined signal with a range square. To increase the signal-to-noise ratio, every 10 data files (each file contains data taken for one minute) are averaged over to give a single 10-minute averaged data. Then, the spatial resolution is determined by averaging over 10 bins (each bin is separated at a distance of 7.5m) spatially to obtain a 75m resolution profile. The RCS is then normalized by calibrating it against theoretical molecular backscatter according to the USSA976 standard atmosphere.

Often, the raw data are contaminated by presence of clouds during data-taking. Such contamination has to be removed so that the data is clean for the purpose of abstracting the values of AOD. LIDAR scattering ratio (defined as LIDAR signal divided by molecular backscatter signal) (Wang and Sassen, 2001; Lo et al., 2006) is used as a means to remove the cloud contaminated data. The referred LIDAR signal here is RCS, whereas molecular backscatter signal is referred to the attenuated molecular backscattering. The backscatter coefficients of the aerosol from LIDAR data are then determined using the method of Fernald (1984).

To strengthen our AOD prediction model, the variability in the retrieved AOD is compared to AOD retrieved from the LIDAR signal. Our LIDAR uses a laser pulse of wavelength 355 nm,

whereas the AERONET data are taken at a different wavelength. A conversion is performed to obtain AOD data from AERONET at 355 nm as described in Eq. (3) using the Angstrom power law (Ångström, 1929). It is used for Angstrom exponent estimation ($\propto$) in terms of AOD (τ_a) measured at wavelength λ_1 = 340 nm and λ_2 =380 nm. In principle, if AOD and Angstrom exponent at one wavelength are known, AOD at a different wavelength can be computed, within the range of validity of Eq. (3), as

$$\propto = -[(\ln\frac{\tau_{a_2}}{\tau_{a_1}}) \div (\ln\frac{\lambda_2}{\lambda_1})] \quad . \tag{3}$$

Therefore, AOD at wavelength 355 nm can be calculated as

$$\tau_{a_{355}} = \tau_{a_{340}} \times (\frac{\lambda_{355}}{\lambda_{340}})^{-\propto} \quad . \tag{4}$$

After the conversions, we repeat the procedure as described above to obtain a new set of coefficients at 355 nm for the AOD predicting model.

Next, an AOD value is obtained from the LIDAR signal. A LIDAR ratio (L) is a constant, defined as the ratio of aerosol extinction coefficient (α_a) and backscatter coefficient (β_a) [see Eq. (5)]. The value of L depends on the particle size distribution, shape and composition. R in Eq. (5) is the range or altitude. α_a can be obtained once β_a and L are known. The value of L has to be assumed for an elastic LIDAR system (Fernald, 1984; He et al., 2006; Lopes et al., 2012). Normally, L values can range from 20-40 sr for clean and polluted marine aerosol particles or dust, urban aerosols (40-60 sr), and biomass burning aerosols (60-80 sr) as suggested by Chew et al. (2013).

$$L(R) = \frac{\alpha_a(R)}{\beta_a(R)} \tag{5}$$

The value of L to be adopted for calculating α_a depends on which dominant aerosol type is in the atmosphere. To arrive at a specific value for L is somewhat arbitrary. Different authors adopt different strategies to fix the value of L. In this study, the following strategy is adopted: the aerosol type is first identified by using a scatter plot of the Angstrom exponent against the AOD (from AERONET data). Once the dominant aerosol type is determined the corresponding L value is set to be the mean value of the range suggested by Chew et al. (2013) for that particular aerosol type. Specifically, for clean and polluted marine aerosol particles or dust, L=30 sr; for urban aerosols, L=50 sr; for biomass burning aerosols, L=70 sr.

AOD values (τ_a) can be obtained using Eq. (6), where R_{max} is the maximum height of the aerosol distribution, and R_0 is the height where the overlap function, O(R) = 1, in our system R_0 is around 200 m. Inaccurate assumption of L can lead to large errors in the retrieval of α_a and τ_a (He et al., 2006), especially under inhomogeneous atmospheric conditions. Therefore, 10 % uncertainty of L and typical values of 7 % uncertainty for β_a are set to estimate potentially erroneous values of α_a at any given R in an atmospheric profile. Finally, all uncertainties in the profile are summed to obtain the uncertainty of the estimated columnar AOD.

$$\tau_a = \int_{R_0}^{R_{max}} \alpha_a(R)dr \tag{6}$$

The LIDAR estimated AOD values obtained were then compared against those predicted by our developed AOD prediction model.

3 Results and discussion

3.1 Climatology of Penang, Malaysia

The climatological results derived from AERONET (http://aeronet.gsfc.nasa.gov/new_web/V2/climo_new/USM_Penang_500.html), based on the work of Holben et al., (2001), for USM Penang are tabulated in Table 1. The monthly AOD (referred to as AOD_500, second column) shows that the two lowest values are 0.18 and 0.19 during the inter-monsoon period (October–November and May). During the southwest monsoon period (June–September), smoke emitted locally and large-scale open burning activities in Sumatra, Indonesia is transported to Malaysia, yielding the highest AOD at approximately 0.31–0.73. However, AOD is 0.21–0.24 during the northeast monsoon period (December–February). Small aerosol particles contribute primarily to the air pollution in Penang, as the average Angstrom exponent for wavelength between 440 nm and 870 nm (referred to as $\text{Angstrom}_{440–870}$) is higher than 1.1. On the other hand, the precipitable water values (referred to as PW) were greater than 4.1, which indicate that Penang has humid atmospheres (Okulov et al., 2002).

3.2 Seasonal variations of AOD, Angstrom exponent, and PW based on frequency distribution patterns

AERONET parameters are plotted (Fig. 1) to reveal the relative frequency distribution at Penang for each seasonal monsoon. Frequency histograms of AOD_500 and $\text{Angstrom}_{440–870}$ (Fig. 1a–b, respectively) indicate changes in the optical properties of aerosols, whereas Fig. 1c shows the amount of water content in the atmospheric column for each season. These histograms here help distinguish aerosol types (Pace et al., 2006; Salinas et al., 2009; Smirnov et al., 2002a, 2011). Our results show that the distributed AOD mainly ranges from 0.2 to 0.4, contributing to approximately 71 % of the total occurrence (Fig. 1a). Fig. 1b shows that the Angstrom exponent is typically between 1.3 and 1.7, translating to ~ 72 % of the total. About 67 % of the total occurrence of PW ranged from 4.5 cm to 5.0 cm (Fig. 1c).

The maximum AOD frequency was centered near 0.2 for all seasons. The clearest season was the post-monsoon (Fig. 1a). Penang was most polluted in the southwest monsoon, most likely due to active open burning activities in Sumatra. The AOD peak was approximately 1.4, with three peaks distributed from AOD_500 = 0.1 to AOD_500 = 1.4 (Fig. 1a). The multiple peaks imply the presence of various aerosol populations, because AOD histograms follow log-normal distribution patterns (Salinas et al., 2009). By contrast, a single peak was observed for the clearest season (post-monsoon).

The frequency distributions as a function of Angstrom exponent display a trend (Fig. 1b) in which approximately 95% of the total occurrence falls within the range of 1 Å to 2 Å. This result implies that the effect of coarse particles (e.g., dust) on the study site was minimal. This statement is supported by Campbell et al. (2013), who showed that dust particles are uncommon in Southeast Asia. However, sometimes dust particle concentrations can be enhanced above the boundary layer. Two noticeable peaks were observed for the Angstrom exponent during the northeast monsoon period (blue curve, Fig. 1b). These aerosols originated

from the northern part of Southeast Asia, particularly Indochina, transported by the monsoon wind and mixed with locally emitted aerosols. Lin et al. (2013) analyzed aerosols in the northern region of Southeast Asia. They found that biomass burning aerosols from Indochina were transported in high- and low-level pathways to the west, and then later shifted to the southwest by northeast monsoons.

Biomass burning aerosols were continuously transported to our study site, as the wind circulation flows toward the southwest direction according to the monthly mean streamline charts of Lin et al. (2013) from 1979 to 2010. During and before the southwest monsoon, Angstrom exponents in Penang ranged between 1.4 and 1.8, indicating the likely presence of biomass burning aerosols (Holben et al., 2001; Gerasopoulos et al., 2003; Toledano et al., 2007). They are likely to originate from local and neighboring countries. Indonesia is known to be very active in open burning during this season. Furthermore, southwest monsoonal winds are likely to have transported these biomass burning aerosols to Penang.

The southwest monsoon period is the driest season in Malaysia. PW frequency was approximately 20 % lower than that of the northeast monsoon period with PW < 4.0 (Fig. 1c). Marked variations in the PW frequency were observed during the northeast monsoon period. Almost no data were obtained for PW < 3.5, except the northeast monsoon period with about 14 % less than this value. The most humid period took place in the post-monsoon, with PW ranging from 5.0 to 5.5 (approximately 74 % of the total occurrence).

3.3 Seasonal discrimination of aerosol types based on the relationship between AOD and Angstrom exponent

Aerosol clusters have been developed using relatively simple scatter plots of AOD and Angstrom exponent. Similar studies have performed this analysis using AERONET data. These datasets have been applied at different locations, such as the Persian Gulf (Smirnov et al., 2002a); several oceanic regions (Smirnov et al., 2002b); Brazil, Italy, Nauru, and Saudi Arabia (Kaskaoutis et al., 2007); Spain (Toledano et al., 2007); Singapore (Salinas et al., 2009); Kuching (Jalal et al., 2012); and the Multi-filter Rotating Shadowband Radiometer in Central Mediterranean (Pace et al., 2006). The scatter plot of $Angstrom_{440–870}$ against AOD_500 or AOD_440 was used to characterize the aerosol type. The wavelength range of $Angstrom_{440–870}$ was used because of its nearness to the typical size range of aerosol based on spectral AOD (Eck et al., 1999). The relation between AOD values at 500 nm and Angstrom 440–870 is commonly used for aerosol classification in scatter plot diagrams (Kaskaoutis et al., 2007). Optically, 500 nm is an effective visible wavelength suitable for aerosol study (Stone, 2002).

Aerosols are classified into five types, including dust, maritime, continental/urban/industrial, biomass burning, and mixed aerosols (Ichoku et al., 2004). Mixed aerosols in practice represent an indistinguishable type that cannot be categorized into any of the previous types. To effectively identify the aerosol distribution types in our study sites, the results are compared using different threshold criteria (Table 2), as presented in Fig. 2.

The thresholds proposed by Pace et al. (2006) and Kaskaoutis et al. (2007) failed to distinguish the maritime aerosol (MA) and dust aerosol (DA). Instead, they show that mixed-type aerosols (MIXA) are dominant at Penang (50–72 %). Urban and industrial (UIA) and biomass burning (BMA) aerosols are grouped into a single class (28–50 % of the total

occurrence). Meanwhile, the threshold suggested by Smirnov et al. (2002b, 2003) failed to identify DA, UIA, and BMA, but efficiently identified MA. As a result, a large amount of MIXA was obtained (> 80 % of the total occurrence). These results reveal the extent of regional uncertainty. Indistinguishable aerosol types in the study sites are significant.

Salinas et al. (2009) suggested that the determination of DA and BMA does not correspond entirely to the range of threshold used in our study, in which the amount of MIXA (approximately 43 % of the total occurrence) was large. Jalal et al. (2012) efficiently identified aerosol types using an alternative threshold criterion. Using their threshold, we find a low amount of MIXA of approximately 21 %. However, the determination of DA was unsatisfactory. The threshold criteria of Toledano et al. (2007) provided the least MIXA (< 5 %; Fig. 2). All thresholds consistently increased from June to September (Fig. 2c), coinciding with the occurrence of haze. UIA was constantly and highly distributed over Penang. Overall, the thresholds provided by Toledano et al. (2007) were selected for our study.

Based on the criteria suggested by Toledano et al. (2007), the UIA class was determined as the highest frequency of occurrence in the overall study period (Fig. 3). This could be the result of Penang being an urban area. The next highest was the MA class, likely due to its geolocation (i.e., surrounded by the sea). BMA is also one of the major pollutants in Penang, which was produced by active burning in local and neighboring countries. These results are consistent with records from our Department of Meteorological, DOE (2010). The study site was minimally affected by DA, which were less than 5 % in each seasonal monsoon. These results are supported by Campbell et al. (2013) who suggest UIA, MA, and BMA are likely the most common aerosol types in Southeast Asia and the maritime continent.

BMA, UIA, and MA obtained in our study during the southwest monsoon were about 45, 24, and 19 %, respectively. During the northeast monsoon period, UIA (approximately 38 %) was the major aerosol in Penang, followed by MA (30 %), BMA (20 %), dust (4 %), and unidentified substances (8 %). However, MIXA reached 17 % in the pre-monsoon, which was the highest among the seasonal monsoons. MA and UIA were 38 %; the MA level was significant during the post-monsoon period (51 %), followed by UIA (40 %) and BMA (< 1 %). The aerosol distribution in Penang is highly seasonally dependent.

3.4 Seasonal flow patterns of air parcels from the HYSPLIT_4 model for identification of aerosol origins

From seven-day seasonal plots of the back-trajectory frequency sourced from the HYSPLIT_4 model, flow patterns reaching the Penang site were determined (Fig. 4) for each monsoon season, averaged between the ground surface up to 5000 m. Residence time analysis was performed to generate the frequency plot and determine the time percentage of a specific air parcel in a horizontal grid cell across the domain.

During the northeast monsoon period, air parcels flow southwestward from the northern part of Southeast Asia (Fig. 4a), including Indochina, through the South China Sea to Penang. Aerosols observed during the northeast monsoon period are also locally produced, whereas those observed during the southwest monsoon period are predominantly from the Andaman Sea, Malacca Strait, and Sumatra (site of open active burning).

Fig. 1b indicates differences in patterns (bimodal distribution pattern) of the seasonal relative

frequency of occurrence for $Angstrom_{440–870}$ during the northeast monsoon compared with the other monsoon periods. These differences are likely attributable to the mixing of various aerosol sources from the northern (e.g., Indochina, Philippines, Taiwan, and eastern China) and southern (e.g., Malaysia and Indonesia) parts of Southeast Asia (refer Fig. 4a). Biomass burning aerosols are likely different for northern and southern SEA because of different types of burning processes (Wardoyo, 2007; Lopes et al., 2012; Bougiatioti et al., 2014; Kaskaoutis et al., 2014). As a result, a bimodal pattern was observed only for the northeast monsoon period (Fig. 1b).

Figure 1b reveals that the distribution patterns of Angstrom exponent between the post-monsoon and northeast monsoon are similar. Figure 4a and d also indicate similarities between the air flow patterns for these monsoon seasons. Hence, a clear correspondence was observed between Fig. 1b with Fig. 4a and d. The similarity in the patterns of Angstrom exponents for the post-monsoon and northeast monsoon may be attributed to the mixture of aerosols from the northern and southern parts of Southeast Asia. Given the classification results (Fig. 3), the occurrence frequency of MA was higher during the post-monsoon and northeast monsoon compared with the southwest and pre-monsoon period. The large amount of MA originates from the South China Sea and Andaman Sea.

For the pre-monsoon period, aerosols observed at Penang originate from the Malacca Strait, Andaman Sea, the northern and some eastern areas of Sumatra, and the western part of peninsular Malaysia, especially the local regions marked in yellow (Fig. 4b). During this season, air flow patterns are similar to those during the southwest monsoon (Fig. 4c). However, a small percentage of aerosols are transported from the northern part of Southeast Asia to Penang during the pre-monsoon period. Indonesia is known to be very active in open burning activities during the southwest monsoon. Therefore the BMA observed in Penang during this season is mainly due to local and transboundary aerosol from Indonesia. This phenomenon is reflected in the narrower and sharper curves on larger values of the Angstrom exponent in Fig. 1b (detailed explanation in Sect. 3.5). A clear correlation is observed between Fig. 1b and Fig. 4b and c during pre-monsoon and southwest monsoon.

The dominant aerosol types are UIA and MA (Fig. 3). The yellow portions in Fig. 4e indicate that for Penang, the second largest city in Malaysia and one of the most industrially-concentrated cities, UIA is a major aerosol type. MA contribution to the overall aerosol distribution is likely influenced by proximity of the surrounding sea.

3.5 Examination of predicted AOD values

The optical properties of aerosol for each monsoonal season are obtained by analyzing the relative frequency occurrence of AOD_500 and $Angstrom_{440–870}$ as shown in Fig. 1a and 1b. We hypothesize that the proposed AOD prediction model should exhibit different accuracies seasonally because the sensitivity for AOD prediction depends on the distribution patterns of the measured AOD; these values were used as inputs to derive the correlation parameters of the model. The sensitivity of AOD prediction is low when the major occurrence frequency is clustered around small AOD values. The insensitivity of the aerosol models to clear atmospheric conditions (e.g., when AOD is low) was also previously observed (Zhong et al., 2007).

Model performance for each monsoonal season was tested (Table 3). The pre-monsoon and

southwest periods exhibited R^2 of 0.65 (RMSE = 0.11) and 0.77 (RMSE = 0.17). However, for the transition period between post-monsoon to northeast monsoon, R^2 values were smaller than 0.45 and RMSE ranged from 0.06 to 0.11. The accuracy of AOD prediction is improved for cases with higher aerosol concentrations. This result is in agreement with the hypothesis mentioned in the previous paragraph. The analysis of twenty two months of data (the so called "overall" model) is satisfactory, with R^2 = 0.72 and RMSE = 0.13. The low value of wMAPE (< 1 %) indicates that the model yielded relatively accurate results for all seasons. Given the criteria that a low wMAPE corresponds with a good prediction, the "overall" dataset yields the least biased prediction. Therefore it is deemed that the "overall" model (which is obtained by training the model using twenty two months of data) can be interpreted as an effective and representative model which can predict AOD in every period.

High correlation was observed between the measured and predicted AOD for the pre-monsoon and southwest monsoon, in which similar air flow patterns occurred (Fig. 4b and c). On the other hand, the prediction accuracy of the AOD model in the post-monsoon and northeast monsoon seasons was moderate. The air flow patterns in Fig. 4a and d, which are associated with northeast and post-monsoons respectively, also show similarity. This observation is consistent with Figure 1b which displays the relative frequencies of occurrence of $\text{Angstrom}_{440-870}$. When scrutinizing the seasonal curves pair by pair, the post-monsoon and northeast monsoon pair (purple and blue curves) appears to be broader and flatter whereas the other two seasons (red and green curves) are sharper and narrower. To be more quantitative, the slopes for the purple and blue pair begin to pick up at a relatively fast pace (compared to the red-green pair) at around Angstrom exponent of 1.1, dropping at around Angstrom exponent of 1.7 from peak values, maintaining a relatively flat profile between these two limits. Whereas the slopes for the red and green pair begin to pick up at a relatively gentle pace (compared to the purple-blue pair) at around Angstrom exponent of 1.1 (for red curve) and 1.3 (for green curve), dropping at around Angstrom exponent of 1.6 (for red curve) and 1.7 (for green curve) from peak values. The profile for the red-green pair is relatively narrower and sharper between their pick-up and dropping limits. As a result, a clear correlation between aerosol optical properties in Fig. 1b and seasonal wind flow patterns in Fig. 4 is observed.

The broader and flatter curves in the post-monsoon and northeast monsoon indicate that coarser aerosols are more frequently loaded in the atmosphere. This observation is proved in Fig. 3, in which both monsoons are showing higher occurrence of MA and lesser BMA in Penang. In fact, we realized that AOD predominantly falls on smaller values if MA is the dominant aerosol type, because clean atmosphere is dominated by MA. When the atmosphere is dominated by UIA then the AOD values are larger than MA. Normally, when BMA is the dominant aerosol type, AOD values are large. In other words, if BMA is absent or small, AOD will have a narrower range of distribution. As a result, only a moderate accuracy in the AOD prediction is obtained for the post-monsoon and northeast monsoon (refer to Table 3).

By comparing the types of dominant aerosol observed during each monsoon, we observe that the results, as obtained in Table 3, correlate well with the information from Fig. 3. Table 3 shows higher coefficients of determination of the proposed AOD prediction model, which can be associated with higher amounts of BMA during the pre-monsoon and southwest monsoon periods. Such observation implies that the aerosol types are possibly indirectly correlated with the AOD prediction model. This result was also noticed by Chen et al. (2013). However, the relationship between the predicted AOD and aerosol type as observed in our model is

qualitative and preliminary. Further study is needed. In addition, as mentioned in Lee at al., (2012) and Gupta et al., (2013), the relationship between AOD and particulate matter at the surface depends also on extent of atmospheric mixing, relative humidity, chemical composition, aerosol size distribution, etc.

3.6 Validation of the predicted AOD

In this subsection the procedure to validate the proposed AOD prediction model is presented. To validate the model accuracy, $\{a_i\}$ was used to generate a set of 'predicted AOD' values that are to be directly compared with those AOD values in data for subset 2. In this case, $\{a_i\}$ are optimized coefficients in Eq. (2); they are obtained from the data for subset 1 of the overall dataset. This set of a_i shall be denoted as 'overall-calibrated $\{a_i\}$. The comparison is shown in Fig. 5. The predicted AOD exhibits a high correlation with the measured AOD (R^2 = 0.68). The temporal characteristics of predictions between 2012 and 2013 are similar to those of the measured AOD. Table 4 shows the performance of the predicted AOD as compared to the measured ones in terms of RMSE and wMAPE. It is found that the RMSE for the predicted AOD is nearly the same as that for the calibration data (as shown in Table 3). Additionally, the error of the validation data is less than 1.0 % in terms of wMAPE (similar accuracy was obtained for the calibration data).

To examine potential bias, the approach proposed by Lee et al. (2012) was performed to remove outliers when the deviation of the predicted AOD was larger than the overall RMSE (0.13). Approximately 21 % of the total data were removed using this method. After filtering, the remaining data were used in the calibration of a_i (this set of a_i shall be denoted as 'overall$_{POR}$-calibrated $\{a_i\}$) in Eq. (2). Note that the values of a_i so obtained are different than that using the original dataset. These two sets of a_i are optimized based on different data sets. R^2 of this fitting increased to 0.92, with RMSE = 0.06 and wMAPE = 0.13 %. The values of R^2, RMSE and wMAPE for the cases with and without outliers removed are shown in Table 3. Thus, by filtering the outliers, R^2 and RMSE were enhanced, but wMAPE only slightly increased from 0.04 % to 0.13 %, although the error value remained less than 1 %. Subsequently, these a_i coefficients (based on the outliers-removed data set) were used to predict AOD, which were then compared against the measured values in data for subset 2 for validation.

In the process of validation, the accuracies of the two sets of AOD values (one set is predicted using $\{a_i\}$ with potential outliers removed, while the other without) are compared, see Table 4. It is found that, in terms of R^2, the AOD predicted using overall$_{POR}$-calibrated $\{a_i\}$ fails to improve when compared to the AOD predicted using overall-calibrated $\{a_i\}$. The wMAPE of AOD prediction before and after filtering the potential outliers are nearly the same. The two sets of AOD predicted can be visually compared in the time series plot in Fig. 5. Such observation implies that the removed data might not be the genuine outliers. In fact the errors were attributed to non uniformly-loaded atmospheric aerosols at different altitudes. We believe that the non-uniform atmospheric mixing caused the high deviations in our predicted results, according to previous studies (Qiu and Yang, 2000; Toth et al., 2014). The proposed model uses ground-based sources as input. It assumes (1) the aerosols are well-mixed, and (2) the air above the planetary boundary layer (PBL) is aerosol free. Any aerosol, if present, above the PBL is not taken into account by the model. If these assumptions are true, the model

can then be correctly compared to the columnar measurement of the sun photometer. However, in reality, aerosol could be present above the PBL, or not always well-mixed, giving rise to some uncertainties in the AOD predicted by the model. These uncertainties are quantified in terms of RMSE.

Figure 5 indicates that most of the predicted AOD values are lower than the measured counterparts. Tan et al. (2014c) analyze the underprediction in these values. They used a LIDAR system to determine the vertical profile of aerosols in Penang and found that the aerosol concentration decreased with height up to the planetary boundary layer (PBL). This layer was less than 2 km during the study period. The large amount of transported aerosols above the boundary layer yielded residual layers (Toth et al., 2014). Significant underestimation of AOD occurred for thick residual layers. By comparing the measured and predicted data in Fig. 5, it is found that only a few small time segments are significantly underpredicted, possibly due to the presence of aerosol residual layers above the PBL. Studies in Cyprus (Retalis et al., 2010) suggest that the extent of atmospheric mixing was relatively homogeneous on scales of a few meters to tens of kilometers. Hence, the predicted results were representative of the large samples. The predicted AOD was underestimated because all measured data were taken from the ground. However, overprediction would be significant if local burning were to occur near the measurement station.

To properly validate the prediction, these data coincide in time with those measured from API, Vis, and AOD level 2. In our case, the LIDAR data coincided only once on 12 July 2013 (Fig. 6). Figure 6a shows the vertical profile of the aerosol backscatter coefficient as a function of time (morning to evening). The brown vertical line represents the instance when both the measured and predicted AOD could be compared with the LIDAR data.

Figure 6b displays the profiles of aerosol backscatter coefficient obtained at 10:00 and 11:00 a.m. local time, respectively. Aerosols had accumulated near the ground at 10:00 a.m. and our model indicated that the predicted AOD was overestimated by 0.039. By contrast, most aerosols at 11.00 a.m. were at a higher level; therefore the model predicted value was underestimated by 0.044. Therefore, the predicted AOD values were acceptable because they exhibited small deviations against the measured AOD. This result was thus valid as long as the aerosols did not considerably differ at altitude levels beneath the planetary boundary layer. The LIDAR data should be therefore considered as an independent validation method for ground-based prediction models.

Aerosols are not always well-mixed in the atmosphere over Penang. Particles transported within the free troposphere are a factor (Toth et al., 2014). If a significant number of elevated aerosol plumes (equivalent to aerosol residual layer) occur over the region, then a large deviation from the predicted value will be produced. Therefore, it can be inferred that a small group of highly underpredicted results (Fig. 5) may be attributed to a significant layer of high-level transported aerosol.

3.7 Applications of the proposed model in the absence of measured AOD data

In this section, we shall apply our AOD-predicting model in the absence of measured AOD data. For the purpose of AOD prediction, the overall-calibrated coefficient $\{a_i\}$, will be used.

The overall$_{POR}$-calibrated coefficient {a_i}, obtained with potential outliers removed, are not used as they may not be genuine outliers, as discussed in Sect. 3.6.

Our proposed model generates AOD data when those from AERONET are unavailable. We described the procedure to predict AOD data. Only the API data for 7.00 a.m., 11.00 a.m., and 5.00 p.m. (local time) were available (http://apims.doe.gov.my) before 24 June 2013. The API data were provided hourly beyond this date. In this study, approximately 5 % of the data were discarded due to fog, rain, or thunderstorms, and only 4493 data points were retained. Figure 7 shows the predicted results from 2012 to 2013, which overlapped with the measured AOD data to simplify the comparison. It is observed that the variation in the predicted AOD matches with that of the measured AOD from AERONET. Hence, as an application of the AOD predicting model, information missed out by sun photometer (i.e., AERONET) could be reasonably well reproduced. These 'retrieved' AOD can be used in other aerosol studies. For example, the diurnal variability of AOD can be significant, depending on location and dominant aerosol type (Arola et al., 2013). They observed that the measurement-based estimates of aerosol direct radiative forcing (also known as aerosol direct radiative effect) at regional or individual sites are substantially influenced by the diurnal variability of AOD. In Pandithurai et al. (2007), they found that the diurnal AOD variation depends on meteorological factors such as relative humidity, winds, temperature and convection activities. Our model provides a helpful means to investigate the uniqueness of diurnal variability of AOD in different seasons of a specific region.

The boxes marked in Fig. 7 are the time windows in which AOD measurements are unavailable. An independent method, i.e., LIDAR is used to estimate AOD at that particular time window (refer to Fig. 8a). In our case, we set L = 70 sr, because this window period is commonly associated with biomass burning aerosol (refer to the relative frequency of dominant of aerosol types in the southwest monsoon, in Fig. 3). Additionally, other studies conducted by Tesche et al. (2011) and Lopes et al. (2012) also suggested L = 70 sr for biomass burning aerosols. Via the procedures as mentioned in Sect. 2, and using the obtained aerosol backscatter coefficient and an assumed L, aerosol extinction coefficients were calculated (based on Eq. 5). Integrating over these aerosol extinction coefficients, AOD values were then estimated using Eq. 6.

If the LIDAR signals were affected by cloud, the AOD data calculated from the LIDAR signal are removed. Then, the predicted AOD from our model and that calculated from LIDAR signal are compared. The result of the comparison between the predicted AOD (by our model) and that derived from LIDAR, as shown in Fig. 8b and c. Fig. 8b, shows that the correlation between these two sets of data is high, as R^2 obtained is 0.86 with RMSE = 0.20. Fig. 8c also indicates that the predicted AOD values from our model are within the error bars of estimated AOD from the LIDAR signal. However, the AOD prediction model is less sensitive during clear atmospheric conditions on 13 Aug (as shown in Fig. 8c).

3.8 Comparison with other linear regression models

The proposed model is compared against other AOD-predicting models from the literature. This is done by comparing the predicted AOD values by our model against the measured AOD in data for subset 1. Table 5 shows the R^2 values of selected AOD-predicting models calculated using the data for subset 1 by our model (Sect. 2). Retalis et al. (2010) suggest

a simple linear regression analysis to predict AOD from the Vis data. Mahowald et al. (2007) suggest a similar linear regression model for the AOD prediction model, in which the Vis data were converted to surface extinction coefficients b_{ext} using the Koschmieder equation Vis = K/b_{ext}, where K (= 3.912) is the Koschmieder constant (Koschmieder, 1924). Two other AOD-predicting models were also compared (Gao and Zha, 2010; Chen et al., 2013).

In these models, linear regression analysis for AOD and PM_{10} was carried out to predict the surface air quality. The approaches can also be used to retrieve AOD after appropriate conversion procedures. Initially, we converted the API data into PM_{10} via the guidance on air pollutant index from DOE (1997). The obtained PM_{10} values were then inputted into the linear regression formula to predict AOD. The linear regressions in these models yielded $R^2 \leq$ 0.6 with RMSE approximately 0.16 and above, which was lower than that of our model ($R^2 \leq$ 0.72 with RMSE = 0.13). wMAPE of these models (0.05 % ~ 0.08 %) were found to be similar but slightly higher than the present model (0.05 %). These figures are reported in Table 5.

4 Conclusions

Seasonal variation in primary aerosol types and their physical characteristics at Penang, Malaysia are analyzed from February 2012 to November 2013. The aerosol types for a specific monsoonal period were determined by applying threshold criteria to scatter plots, in which Angstrom exponent is plotted against aerosol optical depth (AOD). The threshold criteria from Smirnov at al. (2002b, 2003), Pace et at. (2006), Kaskaotis et al. (2007), Toledano et al. (2007), Salinas et al. (2009), and Jalal et al. (2012) were used to distinguish the aerosol types. The testing results indicate that the threshold criteria by Toledano et al. (2007) were the most reliable, because of the minimal occurrence value of the indistinguishable aerosols (referred as mixed-type aerosols, MIXA).

For the study period, biomass burning aerosols (BMA) abruptly increased during the southwest monsoon period, because of active open burning activities in local areas and neighboring countries. During the northeast monsoon period, the optical properties (e.g., size distribution patterns) of the aerosols were unique. Two noticeable peaks were observed in the occurrence frequency of the Angstrom exponents compared with the single peaks for other monsoon seasons. These results were attributed to the mixing of aerosols from local sources with those from the northern part of Southeast Asia, caused by the northeast monsoon winds. Urban and industrial aerosols (UIA) and marine aerosol (MA) were the major aerosols in Penang throughout the year. Dust aerosols (DA) negligibly contributed to the emissions in Penang. The variation in aerosol types for different monsoon seasons clearly yields distinct optical properties.

Previous models have used simple regression analysis between AOD and meteorological parameters to predict the corresponding AOD data. In this study, multiple regression analysis was used in analyzing the proposed model. Two predictors (API and Vis) were introduced to increase statistical reliability. To verify the robustness of multiple regression analysis, in contrast to the simple regression approach, AOD data based on previous simple models were retrieved (Mahowald et al., 2007; Gao and Zha, 2010; Retalis et al., 2010; Chen et al., 2013). R^2, RMSE and wMAPE values in our calibration model are ≤ 0.72, 0.13, 0.05 % respectively. The accuracies are obtained by comparing the predicted AOD values in the current study

against measured AOD in data for subset 1. These figures are compared with the results of other relevant work, which obtained $R^2 \leq 0.60$ and RMSE approximately 0.16 and above. The comparison indicates that the quality of our AOD prediction is statistically better than those simple models, which makes sense given its tuning to local condition.

Predicted AOD from our model are compared with the data derived from a LIDAR system. The values of R^2 and RMSE (0.86 and 0.20) indicate favorable agreement between our model and LIDAR-derived data at wavelength 355 nm. This has added additional weight to the robustness of the developed AOD prediction model.

Our algorithm predicts AOD data during non-retrieval days caused by the frequent occurrence of clouds in the equatorial region. The proposed model yields reliable near real-time AOD data despite the availability of the measured data for limited time points. The predicted AOD data are beneficial for monitoring aerosols in short- and long-term scenarios, their behavior, and provides supplementary information for climatological studies and monitoring aerosol variation.

The technique proposed in this work nevertheless ought to be further stress-tested for the extent of its feasibility by applying it in more cases using a higher volume of data. This technique is pragmatic and cost effective for such environmental study.

Acknowledgements

The authors gratefully acknowledge the financial support provided by RU (grant no. 1001/PFIZIK/811228) and RUI-PRGS grants (grant no. 1001/PFIZIK/846083). The authors would like to thank the members of the NASA Goddard Space Flight Center for setup assembly, as well as the site members who maintained the AERONET in Penang. The authors also acknowledge A. Smirnov from NASA for fruitful discussions on certain issues.

References

Ångström, A.: On the atmospheric transmission of sun radiation and on dust in the air, Geogr. Ann., 11, 156-166, 1929.

Arola, A., Eck, T. F., Huttunen, J., Lehtinen, K. E. J., Lindfors, A. V., Myhre, G., Smirnov, A., Tripathi, S. N., and Yu, H.: Influence of observed diurnal cycles of aerosol optical depth on aerosol direct radiative effect, Atmos. Chem. Phys., 13, 7895-7901, 2013.

Awang, M. B., Jaafar, A. B., Abdullah, A. M., Ismail, M. B., Hassan, M. N., Abdullah, R., Johan, S., and Noor, H.: Air quality in Malaysia: impacts, management issues and future challenges, Respirology, 5, 183–196, 2000.

Bäumer, D., Vogel, B., Versick, S., Rinke, R., Möhler, O., and Schnaiter, M.: Relationship of visibility, aerosol optical thickness and aerosol size distribution in an ageing air mass over South-West Germany, Atmos. Environ., 42, 989–998, doi:10.1016/j.atmosenv.2007.10.017, 2008.

Barladeanu, R., Stefan, S., and Radulescu, R.: Correlation between the particulate matter (PM10) mass concentrations and aerosol optical depth in Bucharest, Romania, Romanian

Reports in Physics, 64, 1085-1096, 2012.

Bougiatioti, A., Stavroulas, I., Kostenidou, E., Zarmpas, P., Theodosi, C., Kouvarakis, G., Canonaco, F., Prévôt, A. S. H., Nenes, A., Pandis, S. N., and Mihalopoulos, N.: Processing of biomass-burning aerosol in the eastern Mediterranean during summertime, Atmos. Chem. Phys., 14, 4793-4807, 2014.

Cachorro, V. E., Vergaz, R., and de Frutos, A. M.: A quantitative comparison of α-Å turbidity parameter retrieved in different spectral ranges based on spectroradiometer solar radiation measurements, Atmos. Environ., 35, 5117–5124, doi:10.1016/S1352-2310(01)00321-1, 2001.

Campbell, J. R., Reid, J. S., Westphal, D. L., Zhang, J., Tackett, J. L., Chew, B. N., Welton, E. J., Shimizu, A., Sugimoto, N., Aoki, K., and Winker, D. M.: Characterizing the vertical profile of aerosol particle extinction and linear depolarization over Southeast Asia and the Maritime Continent: The 2007–2009 view from CALIOP, Atmos. Res., 122, 520-543, doi:http://dx.doi.org/10.1016/j.atmosres.2012.05.007, 2013.

Chen, B. B., Sverdlik, L. G., Imashev, S. A., Solomon, P. A., Lantz, J., Schauer, J. J., Shafer, M. M., Artamonova, M. S., and Carmichael, G.: Empirical relationship between particulate matter and aerosol optical depth over Northern Tien-Shan, Central Asia, Air Qual. Atmos. Health, 6, 385–396, 2013.

Chew, B. N., Campbell, J. R., Reid, J. S., Giles, D. M., Welton, E. J., Salinas, S. V., and Liew, S. C.: Tropical cirrus cloud contamination in sun photometer data, Atmos. Environ., 45, 6724-6731, 2011.

Chew, B. N., Campbell, J. R., Salinas, S. V., Chang, C. W., Reid, J. S., Welton, E. J., Holben, B. N., and Liew, S. C.: Aerosol particle vertical distributions and optical properties over Singapore, Atmos. Environ., 79, 599-613, 2013.

Cordero, L., Wu, Y., Gross, B. M., and Moshary, F.: Use of passive and active ground and satellite remote sensing to monitor fine particulate pollutants on regional scales, in: Advanced Environmental, Chemical, and Biological Sensing Technologies IX, Baltimore, MD, 2012.

de Meij, A., Pozzer, A., Pringle, K. J., Tost, H., and Lelieveld, J.: EMAC model evaluation and analysis of atmospheric aerosol properties and distribution with a focus on the Mediterranean region, Atmos. Res., 114–115, 38–69, 2012.

DOE: A Guide to Air Pollutant Index in Malaysia (API), 3rd Edn., D. O. Environment, Ed., Kuala Lumpur, Malaysia, 1–20, 1997.

DOE: Pollution sources inventory, in: Malaysia Environment Quality Report 2010, ch. 5, Department of Environment, Petaling Jaya, Malaysia, 2010.

Draxler, R. R., and Hess, G. D.: An overview of the HYSPLIT_4 modelling system for trajectories, dispersion and deposition, Aust. Meteorol. Mag., 47, 295-308, 1998.

Eck, T. F., Holben, B. N., Reid, J. S., Dubovik, O., Smirnov, A., O'Neill, N. T., Slutsker, I.,

and Kinne, S.: Wavelength dependence of the optical depth of biomass burning, urban, and desert dust aerosols, J. Geophys. Res.-Atmos., 104, 31333–31349, 1999.

Engling, G., He, J., Betha, R., and Balasubramanian, R.: Assessing the regional impact of Indonesian biomass burning emissions based on organic molecular tracers and chemical mass balance modeling, Atmos. Chem. Phys. Discuss., 14, 2773-2798, 10.5194/acpd-14-2773-2014, 2014.

Fan, X., Chen, H., and Xia, X. a.: Progress in Observation Studies of Atmospheric Aerosol Radiative Properties in China, Chinese J. Atmos. Sci., 37, 477-498, doi:10.3878/j.issn.1006-9895.2012.12316, 2013.

Fernald, F. G.: Analysis of atmospheric lidar observations: some comments, Appl. Optics, 23, 652–653, 1984.

Field, R. D., van der Werf, G. R., and Shen, S. S. P.: Human amplification of drought-induced biomass burning in Indonesia since 1960, Nature Geosci, 2, 185-188, doi:http://www.nature.com/ngeo/journal/v2/n3/suppinfo/ngeo443_S1.html, 2009.

Gao, J. and Zha, Y.: Meteorological influence on predicting air pollution from MODIS-derived aerosol optical thickness: a case study in Nanjing, China, Remote Sens., 2, 2136–2147, 2010.

Gerasopoulos, E., Andreae, M. O., Zerefos, C. S., Andreae, T. W., Balis, D., Formenti, P., Merlet, P., Amiridis, V., and Papastefanou, C.: Climatological aspects of aerosol optical properties in Northern Greece, Atmos. Chem. Phys., 3, 2025–2041, doi:10.5194/acp-3-2025-2003, 2003.

Gupta, P., Khan, M. N., da Silva, A., and Patadia, F.: MODIS aerosol optical depth observations over urban areas in Pakistan: quantity and quality of the data for air quality monitoring, Atmos. Pollut. Res., 4, 43–52, 2013.

Hansen, J., Sato, M., and Ruedy, R.: Radiative forcing and climate response, J. Geophys. Res.-Atmos., 102, 6831–6864, doi:10.1029/96jd03436, 1997.

He, Q. S., Li, C. C., Mao, J. T., Lau, A. K. H., and Li, P. R.: A study on the aerosol extinction-to-backscatter ratio with combination of micro-pulse LIDAR and MODIS over Hong Kong, Atmos. Chem. Phys., 6, 3243-3256, 2006.

Holben, B. N., Eck, T. F., Slutsker, I., Tanré, D., Buis, J. P., Setzer, A., Vermote, E., Reagan, J. A., Kaufman, Y. J., Nakajima, T., Lavenu, F., Jankowiak, I., and Smirnov, A.: AERONET – a federated instrument network and data archive for aerosol characterization, Remote Sens. Environ., 66, 1–16, doi:10.1016/s0034-4257(98)00031-5, 1998.

Holben, B. N., Tanré, D., Smirnov, A., Eck, T. F., Slutsker, I., Abuhassan, N., Newcomb, W. W., Schafer, J. S., Chatenet, B., Lavenu, F., Kaufman, Y. J., Vande Castle, J., Setzer, A., Markham, B., Clark, D., Frouin, R., Halthore, R., Karneli, A., O'Neill, N. T., Pietras, C., Pinker, R. T., Voss, K., and Zibordi, G.: An emerging ground-based aerosol climatology: aerosol optical depth from AERONET, J. Geophys. Res.-Atmos., 106, 12067–

12097, 2001.

Horvath, H.: Estimation of the average visibility in Central Europe, Atmos. Environ., 29, 241–246, doi:10.1016/1352-2310(94)00236-e, 1995.

Hyer, E. J., and Chew, B. N.: Aerosol transport model evaluation of an extreme smoke episode in Southeast Asia, Atmos. Environ., 44, 1422-1427, doi:http://dx.doi.org/10.1016/j.atmosenv.2010.01.043, 2010.

Ichoku, C., Kaufman, Y. J., Remer, L. A., and Levy, R.: Global aerosol remote sensing from MODIS, Adv. Space Res., 34, 820–827, doi:10.1016/j.asr.2003.07.071, 2004.

IPCC: Climate Change 2007: The Physical Science Basis: Contribution of Working Group I to the Fourth Assessment Report of the Intergovernmental Panel on Climate Change, Cambridge University Press, Cambridge, United Kingdom and New York, NY, USA, 2007.

IPCC: Climate Change 2013: The Physical Science Basis: Contribution of Working Group I to the Fifth Assessment Report of the Intergovernmental Panel on Climate Change, Cambridge University Press, Cambridge, United Kingdom and New York, NY, USA, 2013.

Jalal, K. A., Asmat, A., and Ahmad, N.: Retrievals of aerosol optical depth and angstrom exponent for identification of aerosols at Kuching, Sarawak, Trans Tech Publications Inc., Hohhot, China, 5734–5737, 2012.

Kaskaoutis, D. G. and Kambezidis, H. D.: The role of aerosol models of the SMARTS code in predicting the spectral direct-beam irradiance in an urban area, Renew. Energ., 33, 1532–1543, doi:10.1016/j.renene.2007.09.006, 2008.

Kaskaoutis, D. G., Kambezidis, H. D., Hatzianastassiou, N., Kosmopoulos, P. G., and Badarinath, K. V. S.: Aerosol climatology: on the discrimination of aerosol types over four AERONET sites, Atmos. Chem. Phys. Discuss., 7, 6357–6411, doi:10.5194/acpd-7-6357-2007, 2007.

Kaskaoutis, D. G., Kumar, S., Sharma, D., Singh, R. P., Kharol, S. K., Sharma, M., Singh, A. K., Singh, S., Singh, A., and Singh, D.: Effects of crop residue burning on aerosol properties, plume characteristics, and long-range transport over northern India, J. Geophys. Res.-Atmos., 119, 5424-5444, 2014.

Koschmieder, H.: Theorie der horizontalen Sichtweite, Beitr. Phvs. Freien. Atmos., 12, 33–55, 1924.

Krishna Moorthy, K., Suresh Babu, S., and Satheesh, S. K.: Temporal heterogeneity in aerosol characteristics and the resulting radiative impact at a tropical coastal station – Part 1: Microphysical and optical properties, Ann. Geophys., 25, 2293–2308, doi:10.5194/angeo-25-2293-2007, 2007.

Kumar, S. and Devara, P. C. S.: A long-term study of aerosol modulation of atmospheric and surface solar heating over Pune, India, Tellus B, 64, 18420, doi:10.3402/tellusb.v64i0.18420, 2012.

Lee, H. J., Coull, B. A., Bell, M. L., and Koutrakis, P.: Use of satellite-based aerosol optical depth and spatial clustering to predict ambient $PM_{2.5}$ concentrations, Environ. Res., 118, 8–15, 2012.

Li, F. and Lu, D.: Features of aerosol optical depth with visibility grade over Beijing, Atmos. Environ., 31, 3413–3419, doi:10.1016/S1352-2310(97)83211-6, 1997.

Lin, N.-H., Tsay, S.-C., Maring, H. B., Yen, M.-C., Sheu, G.-R., Wang, S.-H., Chi, K. H., Chuang, M.-T., Ou-Yang, C.-F., Fu, J. S., Reid, J. S., Lee, C.-T., Wang, L.-C., Wang, J.-L., Hsu, C. N., Sayer, A. M., Holben, B. N., Chu, Y.-C., Nguyen, X. A., Sopajaree, K., Chen, S.-J., Cheng, M.-T., Tsuang, B.-J., Tsai, C.-J., Peng, C.-M., Schnell, R. C., Conway, T., Chang, C.-T., Lin, K.-S., Tsai, Y. I., Lee, W.-J., Chang, S.-C., Liu, J.-J., Chiang, W.-L., Huang, S.-J., Lin, T.-H., and Liu, G.-R.: An overview of regional experiments on biomass burning aerosols and related pollutants in Southeast Asia: from BASE-ASIA and the Dongsha Experiment to 7-SEAS, Atmos. Environ., 78, 1–19, doi:10.1016/j.atmosenv.2013.04.066, 2013.

Lin, J., van Donkelaar, A., Xin, J., Che, H., and Wang, Y.: Clear-sky aerosol optical depth over East China estimated from visibility measurements and chemical transport modeling, Atmos. Environ., 95, 258-267, 2014a.

Lin, N. H., Sayer, A. M., Wang, S. H., Loftus, A. M., Hsiao, T. C., Sheu, G. R., Hsu, N. C., Tsay, S. C., and Chantara, S.: Interactions between biomass-burning aerosols and clouds over Southeast Asia: Current status, challenges, and perspectives, Environ. Pollut., 2014b.

Lo, C., Comstock, J. M., and Flynn, C.: An atmospheric radiation measurement value-added product to retrieve optically thin cloud visible optical depth using micropulse lidar, Rep. DOE/SC-ARM/TR, 77, 2006.

Lopes, F. J. S., Mariano, G. L., Landulfo, E., and Mariano, E. V. C.: Chapter 9 : Impacts of Biomass Burning in the Atmosphere of the Southeastern Region of Brazil Using Remote Sensing Systems in, edited by: Abdul-Razzak, H., InTech, 247-272, 2012.

Mahowald, N. M., Ballantine, J. A., Feddema, J., and Ramankutty, N.: Global trends in visibility: implications for dust sources, Atmos. Chem. Phys., 7, 3309–3339, doi:10.5194/acp-7-3309-2007, 2007.

Mielonen, T., Portin, H., Komppula, M., Leskinen, A., Tamminen, J., Ialongo, I., Hakkarainen, J., Lehtinen, K. E. J., and Arola, A.: Biomass burning aerosols observed in Eastern Finland during the Russian wildfires in summer 2010 – Part 2: Remote sensing, Atmos. Environ., 47, 279–287, 2012.

Mishra, A. K., Srivastava, A., and Jain, V. K.: Spectral dependency of aerosol optical depth and derived aerosol size distribution over Delhi: An implication to pollution source, Sustain. Environ. Res., 23, 113-128, 2013.

Mogo, S., Cachorro, V. E., and de Frutos, A. M.: In situ UV-VIS-NIR absorbing properties of atmospheric aerosol particles: estimates of the imaginary refractive index and comparison with columnar values, J. Environ. Manage., 111, 267–271, 2012.

Müller, D., Lee, K. H., Gasteiger, J., Tesche, M., Weinzierl, B., Kandler, K., Müller, T., Toledano, C., Otto, S., Althausen, D., and Ansmann, A.: Comparison of optical and microphysical properties of pure Saharan mineral dust observed with AERONET Sun photometer, Raman lidar, and in situ instruments during SAMUM 2006, J. Geophys. Res.-Atmos., 117, D07211 doi:10.1029/2011JD016825, 2012.

Okulov, O., Ohvril, H., and Kivi, R.: Atmospheric precipitable water in Estonia, 1990-2001, Boreal Environ. Res., 7, 291-300, 2002.

Omar, A. H., Won, J.-G., Winker, D. M., Yoon, S.-C., Dubovik, O., and McCormick, M. P.: Development of global aerosol models using cluster analysis of Aerosol Robotic Network (AERONET) measurements, J. Geophys. Res.-Atmos., 110, D10S14, doi:10.1029/2004jd004874, 2005.

Pace, G., di Sarra, A., Meloni, D., Piacentino, S., and Chamard, P.: Aerosol optical properties at Lampedusa (Central Mediterranean). 1. Influence of transport and identification of different aerosol types, Atmos. Chem. Phys., 6, 697–713, doi:10.5194/acp-6-697-2006, 2006.

Pandithurai, G., Pinker, R. T., Devara, P. C. S., Takamura, T., and Dani, K. K.: Seasonal asymmetry in diurnal variation of aerosol optical characteristics over Pune, western India, J. Geophys. Res.-Atmos., 112, 2007.

Peppler, R. A., Bahrmann, C. P., Barnard, J. C., Laulainen, N. S., Turner, D. D., Campbell, J. R., Hlavka, D. L., Cheng, M. D., Ferrare, R. A., Halthore, R. N., Heilman, L. A., Lin, C. J., Ogren, J. A., Poellot, M. R., Remer, L. A., Spinhirne, J. D., Sassen, K., and Splitt, M. E.: ARM Southern Great Plains site observations of the smoke pall associated with the 1998 Central American Fires, B. Am. Meteorol. Soc., 81, 2563–2591, doi:10.1175/1520-0477(2000)081<2563:asgpso>2.3.co;2, 2000.

Qiu, J. and Yang, L.: Variation characteristics of atmospheric aerosol optical depths and visibility in North China during 1980–1994, Atmos. Environ., 34, 603–609, 2000.

Qin, S., Shi, G., Chen, L., Wang, B., Zhao, J., Yu, C., and Yang, S.: Long-term variation of aerosol optical depth in China based on meteorological horizontal visibility observations, Chin. J. Atmos. Sci, 34, 449-456, 2010.

Ramachandran, S. and Srivastava, R.: Influences of external vs. core-shell mixing on aerosol optical properties at various relative humidities, Environm. Sci., 15, 1070–1077, 2013.

Reid, J. S., Hyer, E. J., Johnson, R. S., Holben, B. N., Yokelson, R. J., Zhang, J., Campbell, J. R., Christopher, S. A., Di Girolamo, L., Giglio, L., Holz, R. E., Kearney, C., Miettinen, J., Reid, E. A., Turk, F. J., Wang, J., Xian, P., Zhao, G., Balasubramanian, R., Chew, B. N., Janjai, S., Lagrosas, N., Lestari, P., Lin, N.-H., Mahmud, M., Nguyen, A. X., Norris, B., Oanh, N. T. K., Oo, M., Salinas, S. V., Welton, E. J., and Liew, S. C.: Observing and understanding the Southeast Asian aerosol system by remote sensing: An initial review and analysis for the Seven Southeast Asian Studies (7SEAS) program, Atmos. Res., 122, 403-468, doi:http://dx.doi.org/10.1016/j.atmosres.2012.06.005, 2013.

Retalis, A., Hadjimitsis, D. G., Michaelides, S., Tymvios, F., Chrysoulakis, N., Clayton, C. R. I., and Themistocleous, K.: Comparison of aerosol optical thickness with in situ visibility data over Cyprus, Nat. Hazards Earth Syst. Sci., 10, 421–428, doi:10.5194/nhess-10-421-2010, 2010.

Russell, P. B., Bergstrom, R. W., Shinozuka, Y., Clarke, A. D., DeCarlo, P. F., Jimenez, J. L., Livingston, J. M., Redemann, J., Dubovik, O., and Strawa, A.: Absorption Angstrom Exponent in AERONET and related data as an indicator of aerosol composition, Atmos. Chem. Phys., 10, 1155–1169, doi:10.5194/acp-10-1155-2010, 2010.

Salinas, S. V., Chew, B. N., and Liew, S. C.: Retrievals of aerosol optical depth and Ångström exponent from ground-based Sun-photometer data of Singapore, Appl. Optics, 48, 1473–1484, doi:10.1364/ao.48.001473, 2009.

Salinas, S. V., Chew, B. N., Miettinen, J., Campbell, J. R., Welton, E. J., Reid, J. S., Yu, L. E., and Liew, S. C.: Physical and optical characteristics of the October 2010 haze event over Singapore: A photometric and lidar analysis, Atmos. Res., 122, 555-570, doi:http://dx.doi.org/10.1016/j.atmosres.2012.05.021, 2013.

Sherwood, S., Alexander, M. J., Brown, A., McFarlane, N., Gerber, E., Feingold, G., Scaife, A., and Grabowski, W.: Climate Processes: Clouds, Aerosols and Dynamics, in: Climate Science for Serving Society, edited by: Asrar, G. R., and Hurrell, J. W., Springer Netherlands, 73-103, 2013.

Singh, A. and Dey, S.: Influence of aerosol composition on visibility in megacity Delhi, Atmos. Environ., 62, 367–373, 2012.

Smirnov, A., Holben, B. N., Eck, T. F., Dubovik, O., and Slutsker, I.: Cloud-screening and quality control algorithms for the AERONET database, Remote Sens. Environ., 73, 337–349, doi:10.1016/S0034-4257(00)00109-7, 2000.

Smirnov, A., Holben, B. N., Dubovik, O., O'Neill, N. T., Eck, T. F., Westphal, D. L., Goroch, A. K., Pietras, C., and Slutsker, I.: Atmospheric aerosol optical properties in the Persian Gulf, J. Atmos. Sci., 59, 620–634, doi:10.1175/1520-0469(2002)059<0620:aaopit>2.0.co;2, 2002a.

Smirnov, A., Holben, B. N., Kaufman, Y. J., Dubovik, O., Eck, T. F., Slutsker, I., Pietras, C., and Halthore, R. N.: Optical properties of atmospheric aerosol in maritime environments, J. Atmos. Sci., 59, 501–523, doi:10.1175/1520-0469(2002)059<0501:opoaai>2.0.co;2, 2002b.

Smirnov, A., Holben, B. N., Dubovik, O., Frouin, R., Eck, T. F., and Slutsker, I.: Maritime component in aerosol optical models derived from Aerosol Robotic Network data, J. Geophys. Res.-Atmos., 108, 4033, doi:10.1029/2002jd002701, 2003.

Smirnov, A., Holben, B. N., Giles, D. M., Slutsker, I., O'Neill, N. T., Eck, T. F., Macke, A., Croot, P., Courcoux, Y., Sakerin, S. M., Smyth, T. J., Zielinski, T., Zibordi, G., Goes, J. I., Harvey, M. J., Quinn, P. K., Nelson, N. B., Radionov, V. F., Duarte, C. M., Losno, R., Sciare, J., Voss, K. J., Kinne, S., Nalli, N. R., Joseph, E., Krishna Moorthy, K.,

Covert, D. S., Gulev, S. K., Milinevsky, G., Larouche, P., Belanger, S., Horne, E., Chin, M., Remer, L. A., Kahn, R. A., Reid, J. S., Schulz, M., Heald, C. L., Zhang, J., Lapina, K., Kleidman, R. G., Griesfeller, J., Gaitley, B. J., Tan, Q., and Diehl, T. L.: Maritime aerosol network as a component of AERONET – first results and comparison with global aerosol models and satellite retrievals, Atmos. Meas. Tech., 4, 583–597, doi:10.5194/amt-4-583-2011, 2011.

Song, C., Zaveri, R. A., Alexander, M. L., Thornton, J. A., Madronich, S., Ortega, J. V., Zelenyuk, A., Yu, X.-Y., Laskin, A., and Maughan, D. A.: Effect of hydrophobic primary organic aerosols on secondary organic aerosol formation from ozonolysis of α-pinene, Geophys. Res. Lett., 34, L20803, doi:10.1029/2007gl030720, 2007.

Srivastava, A. K., Singh, S., Tiwari, S., and Bisht, D. S.: Contribution of anthropogenic aerosols in direct radiative forcing and atmospheric heating rate over Delhi in the Indo-Gangetic Basin, Environ. Sci. Pollut. R., 19, 1144–1158, 2012.

Stone, R. S.: Monitoring aerosol optical depth at Barrow, Alaska and South Pole; historical overview, recent results, and future goals, in: Proceedings of the 9th Workshop Italian Research on Antarctic Atmosphere, 22–24 October 2001, Rome, Italy, 123–144, 2002.

Suresh Babu, S., Krishna Moorthy, K., and Satheesh, S. K.: Temporal heterogeneity in aerosol characteristics and the resulting radiative impacts at a tropical coastal station – Part 2: Direct short wave radiative forcing, Ann. Geophys., 25, 2309–2320, doi:10.5194/angeo-25-2309-2007, 2007.

Tan, F., Abdullah, K., Lim, H. S., MatJafri, M. Z., Welton, E. J., and Lolli, S.: An initial assessment of ground based lidar backscattered signal in Penang Island, in: IEEE International Conference on Space Science and Communication (IconSpace) 2013, Melaka, Malaysia, 1–3 July 2013, 228–232, 2013.

Tan, F., Lim, H. S., Abdullah, K., Yoon, T. L., Matjafri, M. Z., and Holben, B.: Multiple regression method to determine aerosol optical depth in atmospheric column in Penang, Malaysia, IOP C. Ser. Earth Env., 18, 012081, doi:10.1088/1755-1315/18/1/012081, 2014a.

Tan, F., Lim, H. S., Abdullah, K., Yoon, T. L., Matjafri, M. Z., and Holben, B.: Manipulating API and AOD data to distinguish transportation of aerosol at high altitude in Penang, Malaysia, IOP C. Ser. Earth Env., 18, 012082, doi:10.1088/1755-1315/18/1/012082, 2014b.

Tan, F. Y., Hee, W. S., Hwee, S. L., Abdullah, K., Tiem, L. Y., Matjafri, M. Z., Lolli, S., Holben, B., and Welton, E. J.: Variation in daytime troposphereic aerosol via LIDAR and sunphotometer measurements in Penang, Malaysia, AIP Conference Proceedings, 1588, 286–292, doi:10.1063/1.4866962, 2014c.

Tang, I. N.: Chemical and size effects of hygroscopic aerosols on light scattering coefficients, J. Geophys. Res.-Atmos., 101, 19245–19250, doi:10.1029/96jd03003, 1996.

Tesche, M., Gross, S., Ansmann, A., MÜLler, D., Althausen, D., Freudenthaler, V., and Esselborn, M.: Profiling of Saharan dust and biomass-burning smoke with multiwavelength

polarization Raman lidar at Cape Verde, Tellus B, 63, 649-676, doi:10.1111/j.1600-0889.2011.00548.x, 2011.

Tesfaye, M., Botai, J., Sivakumar, V., and Mengistu Tsidu, G.: Evaluation of Regional Climatic Model Simulated Aerosol Optical Properties over South Africa Using Ground-Based and Satellite Observations, ISRN Atmos. Sci., 2013, 17, doi:10.1155/2013/237483, 2013.

Toledano, C., Cachorro, V. E., Berjon, A., de Frutos, A. M., Sorribas, M., de la Morena, B. A., and Goloub, P.: Aerosol optical depth and Ångström exponent climatology at El Arenosillo AERONET site (Huelva, Spain), Q. J. Roy. Meteor. Soc., 133, 795–807, doi:10.1002/qj.54, 2007.

Toth, T. D., Zhang, J., Campbell, J. R., Hyer, E. J., Reid, J. S., Shi, Y., and Westphal, D. L.: Impact of data quality and surface-to-column representativeness on the PM2.5/satellite AOD relationship for the contiguous United States, Atmos. Chem. Phys., 14, 6049-6062, 2014.

Tripathi, S. N., Dey, Sagnik, Chandel, A., Srivastava, S., Singh, Ramesh P., and Holben, B. N.: Comparison of MODIS and AERONET derived aerosol optical depth over the Ganga Basin, India, Ann. Geophys., 23, 1093–1101, doi:10.5194/angeo-23-1093-2005, 2005.

van Beelen, A. J., Roelofs, G. J. H., Hasekamp, O. P., Henzing, J. S., and Röckmann, T.: Estimation of aerosol water and chemical composition from AERONET Sun–sky radiometer measurements at Cabauw, the Netherlands, Atmos. Chem. Phys., 14, 5969–5987, doi:10.5194/acp-14-5969-2014, 2014.

Wai, K. M., Wu, S., Kumar, A., and Liao, H.: Seasonal variability and long-term evolution of tropospheric composition in the tropics and Southern Hemisphere, Atmos. Chem. Phys., 14, 4859-4874, 2014.

Wang, J. and Christopher, S. A.: Intercomparison between satellite-derived aerosol optical thickness and $PM_{2.5}$ mass: implications for air quality studies, Geophys. Res. Lett., 30, 2095, doi:10.1029/2003gl018174, 2003.

Wang, K., Dickinson, R. E., and Liang, S.: Clear Sky Visibility Has Decreased over Land Globally from 1973 to 2007, Science, 323, 1468-1470, doi:10.1126/science.1167549, 2009.

Wang, Z., Liu, Y., Hu, M., Pan, X., Shi, J., Chen, F., He, K., Koutrakis, P., and Christiani, D. C.: Acute health impacts of airborne particles estimated from satellite remote sensing, Environ. Int., 51, 150–159, 2013.

Wang, Z., and Sassen, K.: Cloud type and macrophysical property retrieval using multiple remote sensors, J. Appl. Meteor., 40, 1665-1682, 2001.

Wardoyo, A. Y.: Biomass burning : particle emissions, characteristics, and airborne measurements PhD, Faculty of Science, Queensland University of Technology, Queensland University of Technology, 257 pp., 2007.

Xian, P., Reid, J. S., Atwood, S. A., Johnson, R. S., Hyer, E. J., Westphal, D. L., and Sessions, W.: Smoke aerosol transport patterns over the Maritime Continent, Atmos. Res.,

122, 469–485, doi:10.1016/j.atmosres.2012.05.006, 2013.

Zhong, B., Liang, S., and Holben, B.: Validating a new algorithm for estimating aerosol optical depths over land from MODIS imagery, Int. J. Remote Sens., 28, 4207–4214, 2007.

Tables

Table 1. Average values of model-related parameters from the database collected from November 2011 to November 2013 in USM Penang (latitude, 05°21′ N; longitude, 100°18′ E; elevation, 51 m).

Month	AOD_500	sigma AOD_500	Angstrom 440–870	sigma Angstrom 440–870	PW	sigma PW	*N*	Number of Month
JAN	0.24	0.09	1.33	0.18	4.19	0.47	21	1
FEB	0.21	0.09	1.39	0.23	4.44	0.58	18	2
MAR	0.36	0.16	1.41	0.19	4.15	0.58	31	2
APR	0.32	0.19	1.42	0.16	4.78	0.53	29	2
MAY	0.19	0.07	1.10	0.33	4.48	0.43	11	2
JUN	0.48	0.35	1.30	0.33	4.56	0.37	14	2
JUL	0.31	0.18	1.39	0.21	4.50	0.49	14	2
AUG	0.73	0.39	1.50	0.19	4.58	0.25	13	1
SEP	0.35	0.23	1.40	0.17	4.78	0.45	14	2
OCT	0.19	0.08	1.31	0.19	4.48	0.32	16	2
NOV	0.18	0.07	1.31	0.20	4.72	0.41	24	3
DEC	0.21	0.04	1.41	0.20	4.67	0.27	8	1
YEAR	0.31	0.16	1.36	0.10	4.53	0.20	213	22

Table 2. Threshold values of AOD and Angstrom$_{440–870}$ for aerosol classification. Abbreviations: MA = maritime, DA = dust, UIA = urban and industrial, BMA = biomass burning, MIXA = mixed-type aerosols. MIXA represents indistinguishable aerosol type that lies beyond the threshold ranges.

	Jalal et al. (2012)		**Toledano et al. (2007)**		**Salinas et al. (2009)**		**Pace et at. (2006) and D. Kaskaotis (2007)**		**Smirnov (2002b, 2003)**	
Aerosol Type	**Angstrom$_{440–870}$**	**AOD 440**	**Angstrom$_{440–870}$**	**AOD 440**	**Angstrom$_{440–870}$**	**AOD 500**	**Angstrom$_{440–870}$**	**AOD 500**	**Angstrom$_{440–870}$**	**AOD 500**
MA	0.5–1.7	≤ 0.3	0–2	≤ 0.2	0.5–1.7	≤ 0.15	≤ 1.3	≤ 0.06	≤ 1.0	≤ 0.15
DA	≤ 1.0	≥ 0.4	≤ 1.05	≥ 0.11 (only this value is for AOD_870)	≤ 1.0	≥ 0.4	≤ 0.5	≥ 0.15	≤ 0.7	≥ 0.2
UIA	≥ 1.0	0.2–0.4	≥ 1.05	0.2–0.35	≥ 1.0	0.2–0.4	≥ 1.5	≥ 0.1	≥ 1.5	≥ 0.4
BMA	≥ 1.0	≥ 0.7	≥ 1.4	≥ 0.35	≥ 1.0	≥ 0.8				

Table 3. Calibration results (data for subset 1) for the AOD prediction model [**Eq. (2)**] from 2012 and 2013 data.

Monsoon	R^2	RMSE	wMAPE (%)	N
Northeast monsoon	0.41	0.11	0.40	129
Pre-Monsoon	0.64	0.11	0.37	65
Southwest monsoon	0.77	0.17	0.08	117
Post-monsoon	0.42	0.06	0.21	83
Overall	0.72	0.13	0.04	394
Overall $_{POR}$	0.92	0.06	0.13	307

Note: POR = potential outliers removed, N = number of data

Table 4. Validation results (data for subset 2) for the AOD prediction model [**Eq. (2)**] from 2012 and 2013 data.

	R^2	RMSE	wMAPE (%)	N
Overall (using overall-calibrated $\{a_i\}$)	0.68	0.14	0.05	395
Overall (using overall$_{POR}$-calibrated $\{a_i\}$)	0.68	0.14	0.03	395

Note: POR = potential outliers removed, N = number of data

Table 5. R^2 values of the AOD predicted by selected linear regression models from the literature. The values of R^2, RMSE and wMAPE shown in this table are obtained by comparing the predicted AOD values against measured AOD data from subset 1.

Model	Author(s)	R^2	RMSE	wMAPE (%)
$\mathbf{AOD = a_0 + a_1(Vis)}$	(Retalis et al., 2010)	0.56	0.17	0.08
$\mathbf{AOD = a_0 + a_1(b_{ext})}$	(Mahowald et al., 2007)	0.58	0.17	0.07
$\mathbf{AOD = a_0 + a_1(PM10)}$	(Gao and Zha, 2010;Chen et al., 2013)	0.60	0.16	0.05
$\mathbf{AOD = a_0 + a_1(Vis) + a_2(Vis)^2 + a_3(Vis)^3 + a_4(API) + a_5(API)^2 + a_6(API)^3}$	Current Study	0.72	0.13	0.05

Figures

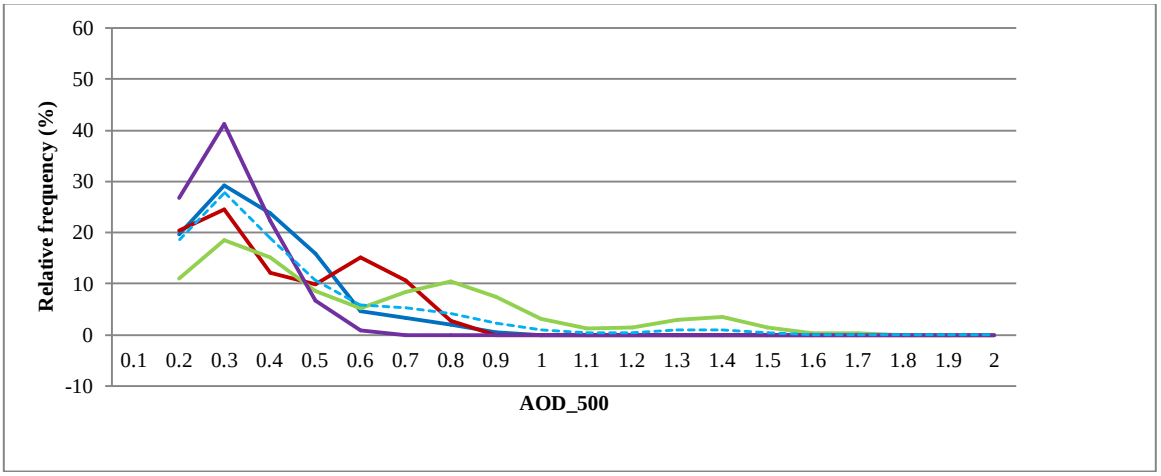

a)

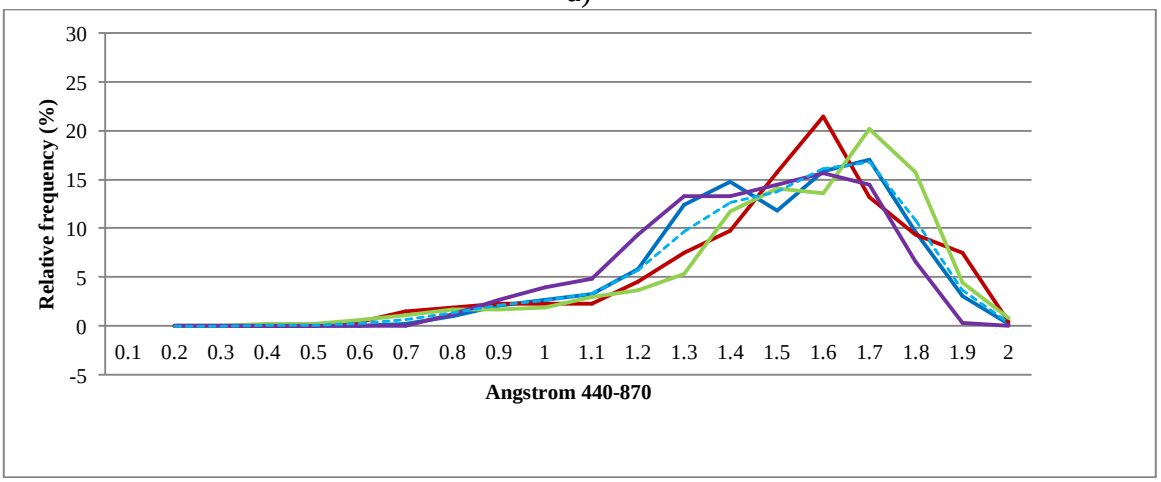

b)

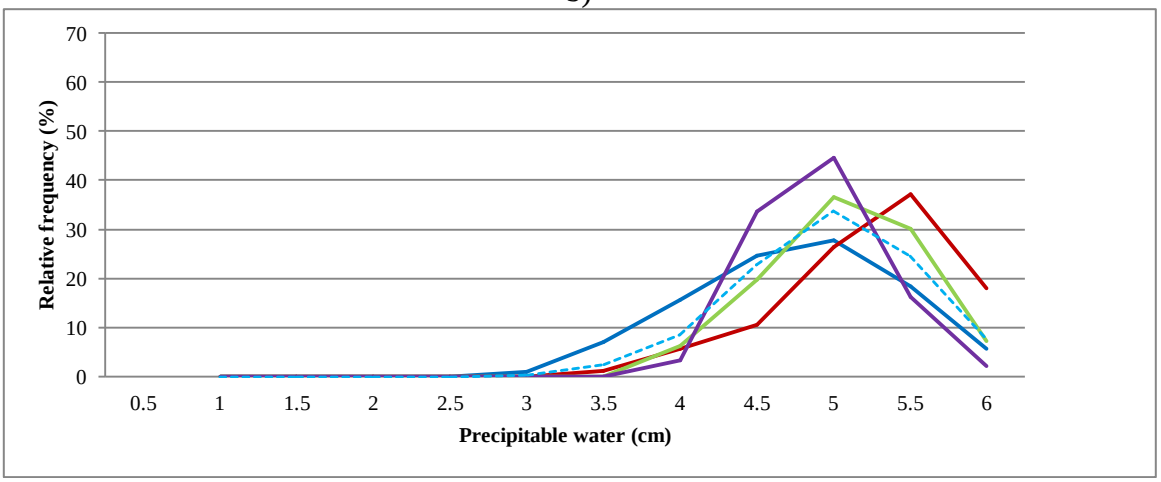

c)

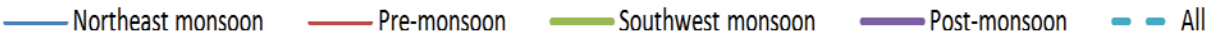

Figure 1. Seasonal relative frequencies of occurrences of (a) AOD_500, (b) Angstrom$_{440–870}$, and (c) PW in Penang for February 2012 to November 2013. Each curve was smoothed by using a moving average technique.

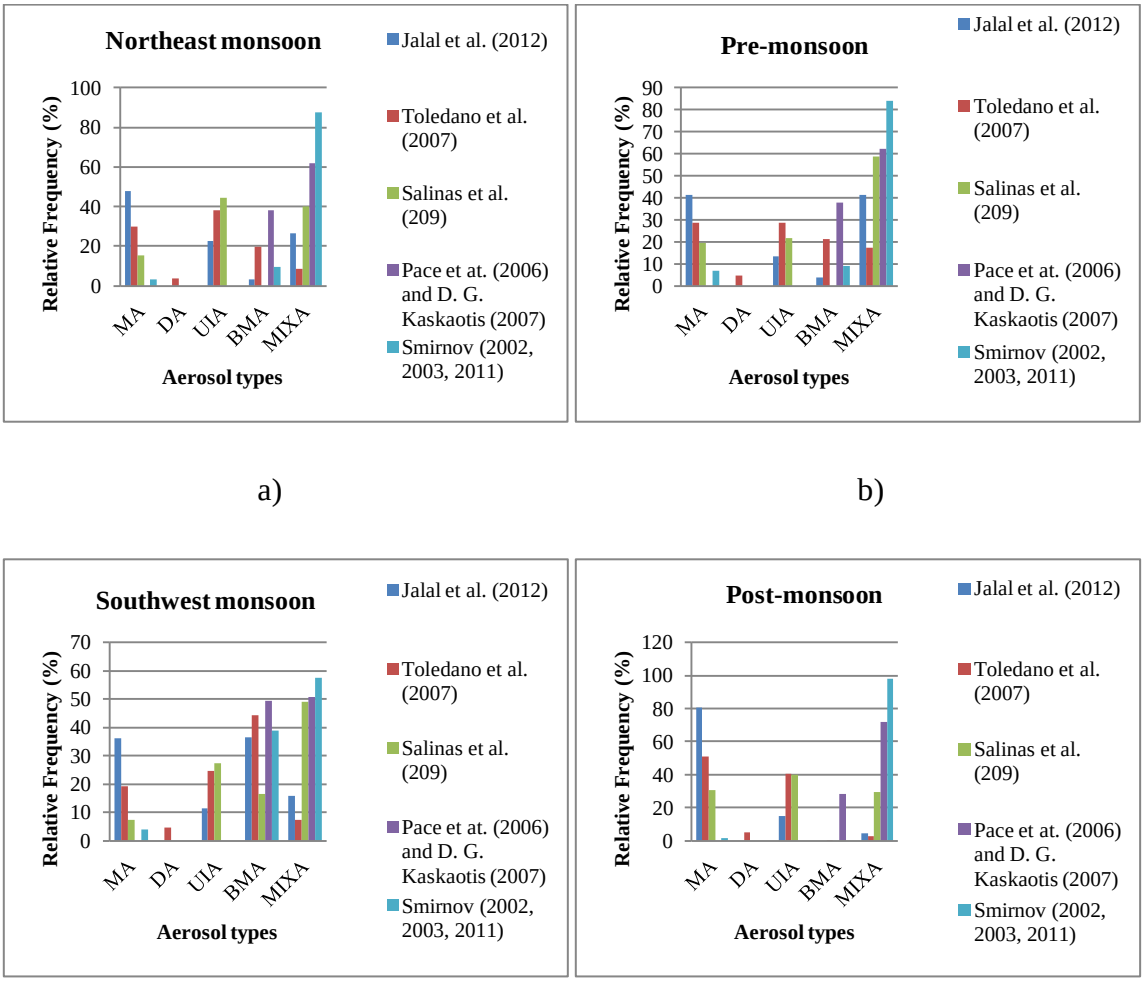

a) b)

c) d)

Figure 2. Classification of aerosol types for a) December–March, b) April–May, c) June–September, and d) October–November based on AOD–Angstrom$_{440–870}$ scatter plots by proposed thresholds.

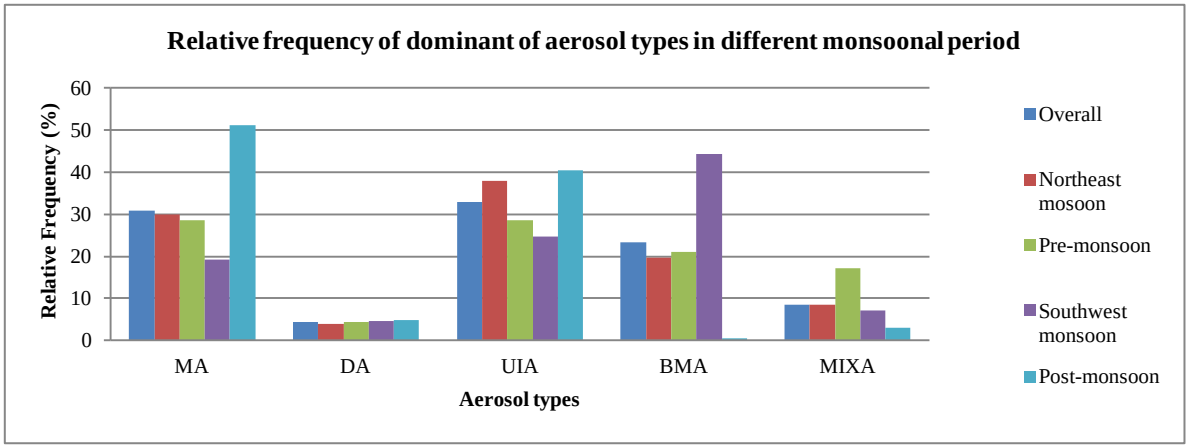

Figure 3. Seasonal classification of aerosol types based on AOD–Angstrom$_{440–870}$ scatter plots by the threshold proposed by Toledano et al. (2007).

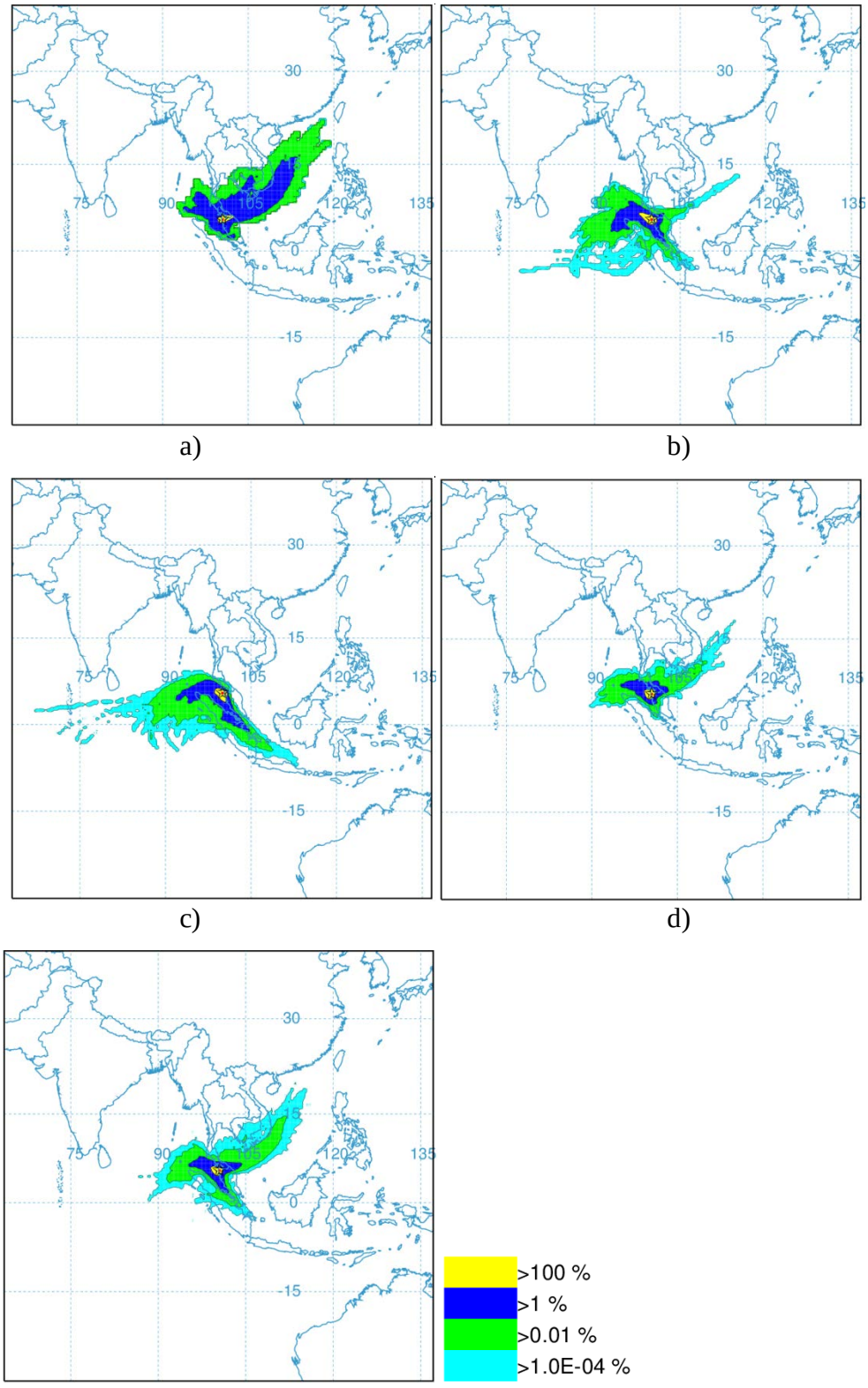

Figure 4. Seasonal back-trajectory frequency plot by the HYSPLIT_4 model (Draxler and Hess, 1998) for a) northeast monsoon, b) pre-monsoon, c) southwest monsoon, d) post-monsoon, and e) overall study period at

Penang, which was marked as a five-edged star (5.50˚ N and 100.50˚ E, from altitude 51 m).

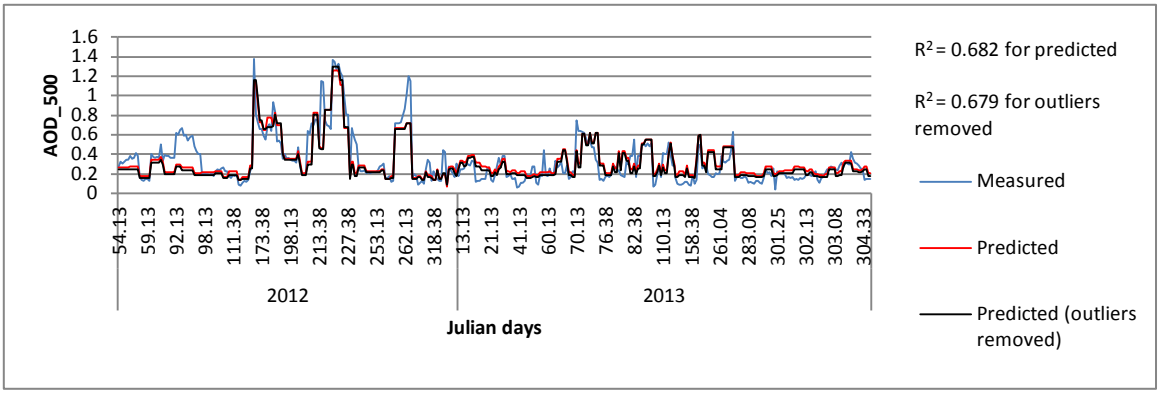

Figure 5. Predicted and measured AOD at 500 nm for 2012 and 2013 for validation dataset (subset 2, with 395 data points). The plot in black are predicted AOD values using $\{a_i\}$ obtained dataset with potential outliers removed, whereas that in red is with dataset without removing potential outliers.

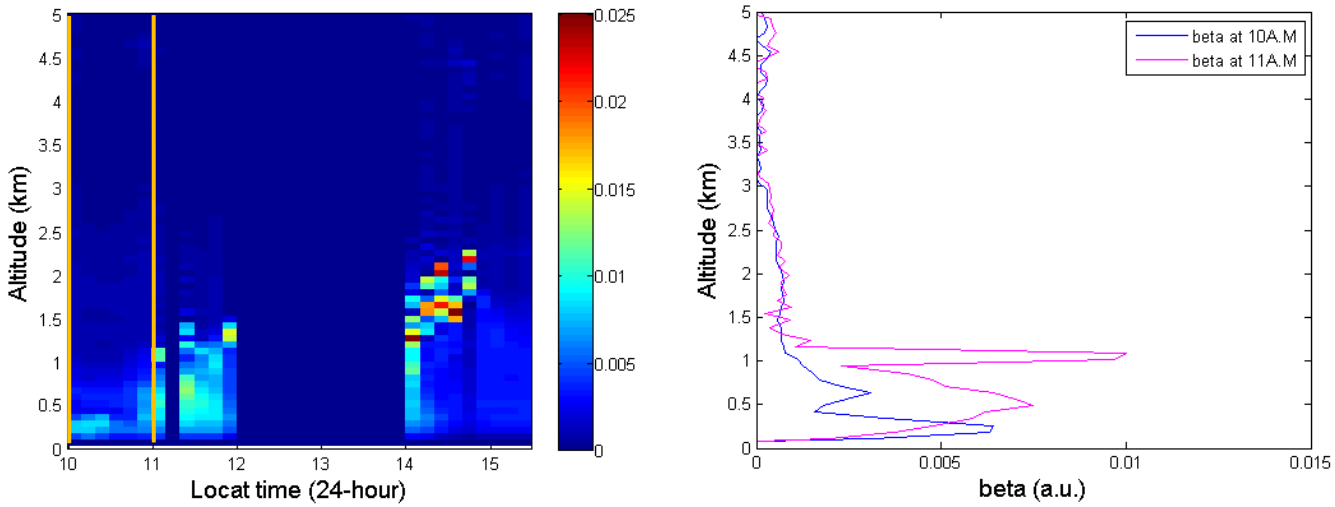

a) b)

Figure 6. a) Profiles of the aerosol backscatter coefficients ($km^{-1}sr^{-1}$) recorded on 12 July 2013. No data were acquired from 12 PM to 2 PM. The brown lines represent the moment of acquisition of sun photometer; b) profiles of the aerosol backscatter coefficient (beta) obtained from 10 AM to 11 AM for the brown lines in a).

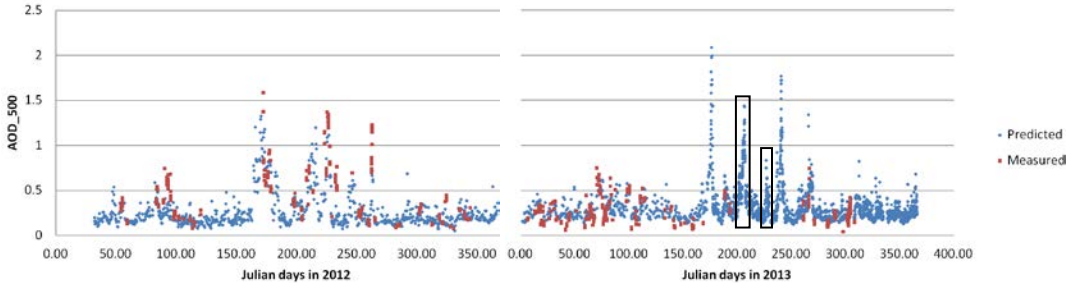

Figure 7. Predicted AOD_500 data plotted against the period from 2012 to 2013 (input all Vis and API available data into the established model to predict AOD, with 4493 data points). Rectangles 1 and 2 correspond to the data recorded on 24–25 July and 13–14 August 2013, respectively. These data were used for comparison with those obtained from LIDAR (**Fig. 8**).

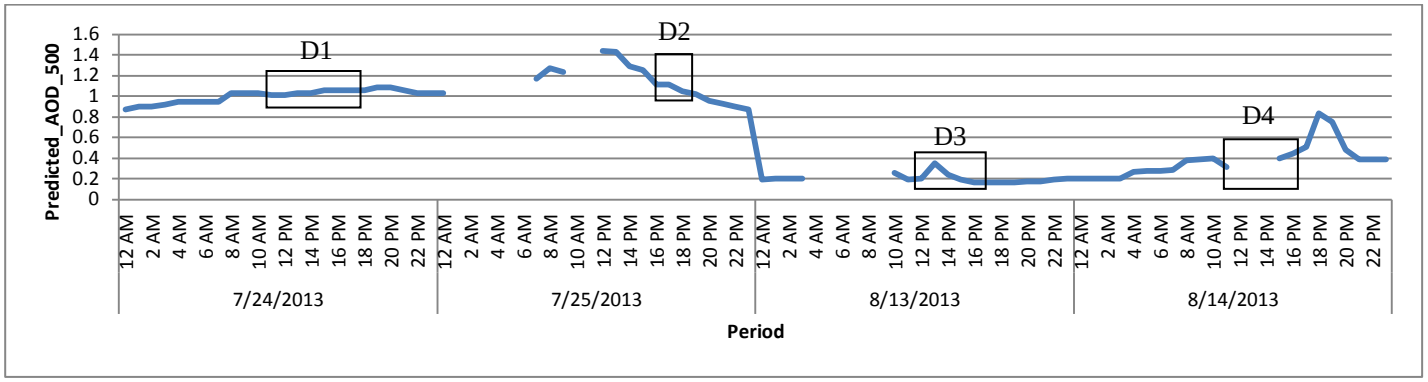

a)

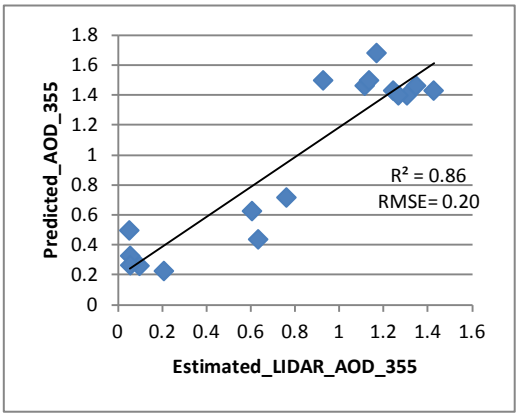

b)

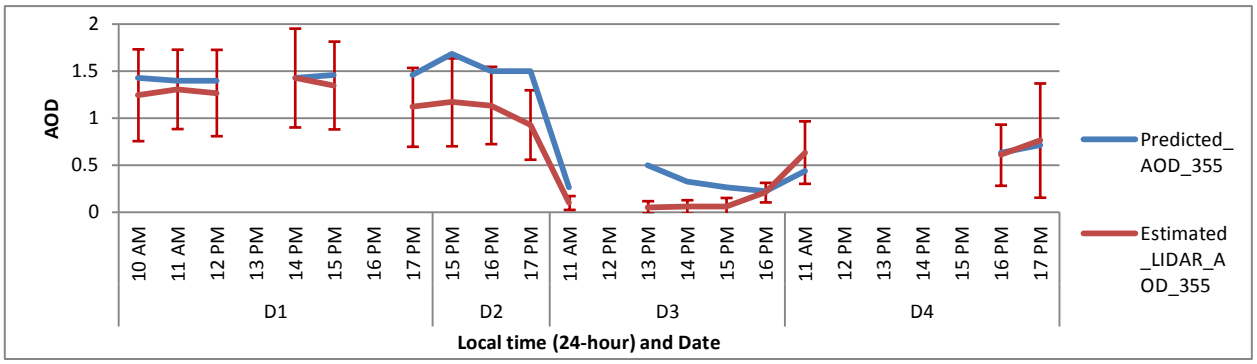

c)

Figure 8. a) Hourly retrieved AOD recorded on a) 24–25 July and 13–14 August 2013 (the gaps are due to fog, rain, or when API value is predominantly caused by O_3 but not PM_{10}). b) A scatter plot for AOD_355 predicted from our model versus the AOD calculated from Raymetrics LIDAR system. c) Predicted AOD from our model and estimated AOD from LIDAR plotted versus local time and date (the gaps indicate no data available at the particular time due to LIDAR system was switched off or cloud contamination above the LIDAR system). Error bars for estimated AOD from LIDAR are shown.